1	Comparison of three radar-based precipitation nowcasts for the extreme
2	July 2021 flooding event in Germany
3	
4	Mohamed Saadi ^{a,b,c} , Carina Furusho-Percot ^{a,b,d} , Alexandre Belleflamme ^{a,b} , Silke Trömel ^{e,f} ,
5	Stefan Kollet ^{a,b} , and Ricardo Reinoso-Rondinel ^{e,g,h}
6	^a Institute of Bio- and Geosciences (IBG-3, Agrosphere), Forschungszentrum Jülich, Jülich, Germany
7 8	^b Centre for High-Performance Scientific Computing in Terrestrial Systems, Geoverbund ABC/J, Jülich, Germany
9 10	° Institut de Mécanique des Fluides de Toulouse (IMFT), Université de Toulouse, CNRS-INPT-UPS, Toulouse France
11	d US 1116 AGROCLIM, INRAE Centre de Recherche PACA, Avignon, France
12	^e Institute for Geosciences, Department of Meteorology, Universität Bonn, Bonn, Germany
13	^f Laboratory for Clouds and Precipitation Exploration, Geoverbund ABC/J, Bonn, Germany
14 15	^g Faculty of Engineering Science, Department of Civil Engineering, Katholieke Universiteit Leuven, Leuven, Belgium
16 17	^h Department of Meteorological Observations and Research, Royal Meteorological Institute of Belgium, Brussels, Belgium
18	
19	Corresponding author: Mohamed Saadi, mohamed.saadi@toulouse-inp.fr
20	Accepted for publication on 14 April 2023 in Journal of Hydrometeorology, DOI:
21	https://doi.org/10.1175/JHM-D-22-0121.1

22 ABSTRACT

23	Quantitative precipitation nowcasts (QPN) can improve the accuracy of flood forecasts
24	especially for lead times up to 12 hours, but their evaluation depends on a variety of factors,
25	namely the choice of the hydrological model and the benchmark. We tested three
26	precipitation nowcasting techniques based on radar observations for the disastrous mid-July
27	2021 event in seven German catchments (140-1670 km²). Two deterministic [advection-
28	based and Spectral Prognosis (S-PROG)] and one probabilistic [Short-Term Ensemble
29	Prediction System (STEPS)] QPN with maximum lead time of 3 h were used as input to two
30	hydrological models: a physically-based, 3D-distributed model (ParFlowCLM) and a
31	conceptual, lumped model (GR4H). We quantified the hydrological added value of QPN
32	compared with hydrological persistence and zero-precipitation nowcasts as benchmarks. For
33	the 14 July 2021 event, we obtained the following key results: (1) According to the quality of
34	the forecasted hydrographs, exploiting QPN improved the lead times by up to 4 h (8 h)
35	compared with adopting zero-precipitation nowcasts (hydrological persistence) as a
36	benchmark. Using a skill-based approach, obtained improvements were up to 7-12 h
37	depending on the benchmark. (2) The three QPN techniques obtained similar performances
38	regardless of the applied hydrological model. (3) Using zero-precipitation nowcasts instead of
39	hydrological persistence as benchmark reduced the added value of QPN. These results
10	highlight the need for combining a skill-based approach with an analysis of the quality of
11	forecasted hydrographs to rigorously estimate the added value of QPN.
12	Keywords: Extreme events; Ensembles; Nowcasting; Hydrologic models; Model
13	evaluation/performance; Flood events
14	1. Introduction
15	Precipitation extremes are intensifying due to human-driven climate change (Fowler et al.
16	2021). This means more severe and more frequent flooding events, which will lead to costlier
17	damages to infrastructures and heavier human losses (Dottori et al. 2018; Dougherty and
18	Rasmussen 2020). To mitigate these damages, operational and efficient flood warning
19	systems are needed more than ever (Pappenberger et al. 2015a). These provide flood
50	forecasts by relying on hydrological models fed with meteorological forecasts from
51	numerical weather prediction (NWP) systems (Alfieri et al. 2012; Cloke and Pappenberger
52.	2009) With ensemble modeling data assimilation, and improved representation of physical

- processes enabled by the development of convection-permitting schemes (Speight et al. 2021;
- Clark et al. 2016), the skill of NWP has significantly increased during the last decades (Bauer
- et al. 2015), making it the best input for flood forecasting at the regional scale and for long
- horizons (> 6h; Lin et al., 2005). However, their use for short lead times (< 6h) in small-scale
- 57 applications (enabled by using convection-permitting NWP) is hindered by the time needed
- for their spin-up and their too coarse spatial resolution for hydrological needs.
- 59 Statistical extrapolation of the up-to-date weather radar observations (or nowcasting) can
- fill this gap by providing quantitative precipitation nowcasts (QPN) at high spatial and
- 61 temporal resolutions (up to 1 km² and 5 min, respectively; see for example Reinoso-Rondinel
- et al. 2022), which can outperform the NWP for short lead times (Berenguer et al. 2012). This
- 63 level of detail is particularly useful to forecast flash floods from convective precipitation
- events especially in urban areas and rapidly responding catchments (Berenguer et al. 2005;
- Foresti et al. 2016; Ochoa-Rodriguez et al. 2015). Most QPN are generated by (1) estimating
- the motion field from remote sensing products, such as radar or satellite images, and (2)
- applying this motion field to displace the most recently observed precipitation field (Ayzel et
- al. 2019). These two steps form the core of most deterministic nowcasting techniques such as
- 69 TREC (Tracking Radar Echo with Correlations, Rinehart and Garvey 1978), MAPLE
- 70 (McGill Algorithm for Precipitation nowcasting by Lagrangian Extrapolation; Germann and
- 71 Zawadzki 2002), S-PROG (Spectral Prognosis; Seed 2003), and SWIRLS (Short-range
- Warning of Intense Rainstorms in Localized Systems; Woo and Wong 2017). To account for
- uncertainties in the motion field as well as in the evolution of the precipitation cells, many
- techniques adopt a stochastic approach by adding random perturbations based on
- 75 corresponding spatiotemporal properties to produce an equally likely ensemble of QPN.
- 76 Examples of these probabilistic techniques include STEPS (Bowler et al. 2006), STEPS-BE
- 77 (STEPS system for Belgium; Foresti et al. 2016), SBMcast (String of Beads model;
- 78 Berenguer et al. 2011), and ENS (Sokol et al. 2017).
- 79 To evaluate the skill of QPN, several studies quantified the ability of nowcasting
- 80 techniques to provide accurate short-term predictions of observed precipitation (see Table 1;
- Berenguer et al. 2011; Atencia and Zawadzki 2014, 2015; Mejsnar et al. 2018; Imhoff et al.
- 82 2020; Reinoso-Rondinel et al. 2022). Their approach compares the predicted precipitation
- 83 from QPN for a given lead time with quantitative precipitation estimates (QPE) obtained
- 84 from radar observations. These studies focused on improving the nowcasting methods to

account for uncertainties in the prediction of precipitation fields and highlighted the limits of the applied methods in the case of warm-season and convective events (Mejsnar et al. 2018). To characterize and enhance the hydrological predictability of associated flash floods, Imhoff et al. (2020) analyzed the effect of catchment properties and event characteristics (such as the size and location) on the nowcasting skill. Towards a nationwide nowcasting system, Reinoso-Rondinel et al. (2022) improved the S-PROG technique by introducing spatially localized parameters for the inherent auto-regressive model and evaluated the skill with respect to radar-based QPE for 10 observed rain events in Germany.

An alternative evaluation framework exploits (ensemble) QPN to serve as input to a hydrological model (see Table 1; Šálek et al. 2006; Berenguer et al. 2005; Vivoni et al. 2006; Xuan et al. 2014; Heuvelink et al. 2020; Lovat et al. 2022; Imhoff et al. 2022). The resulting simulated discharge time series are then compared to a reference discharge time series, which can be either the observed discharge, if available, or the simulated discharge by the hydrological model with QPE (i.e., observed precipitation) as input precipitation. This framework is more relevant for flood forecasting applications since it quantifies the added value of QPN, with respect to e.g. zero-precipitation nowcasts, in improving the lead time of hydrological forecasts. All studies found that radar-based QPN enhanced the forecasting skill achieved by the hydrological model, especially when blended with NWP forecasts (Lovat et al. 2022). Moreover, the forecasting skill depended on the physical properties of the catchment (such as size and topography), the type of the event (convective vs. stratiform), and the season (rain vs. snow).

Reference	QPN method	Location	Hydrological model
Berenguer et al.	SBMcast	Barcelona, Spain	_
(2011)	(probabilistic)		
Atencia and Zawadzki	Two probabilistic	United States	_
(2014, 2015)	nowcasting methods		
Mejsnar et al. (2018)	COTREC	Czech Republic	_
	(deterministic; Li et al.		
	1995)		
Imhoff et al. (2020)	Four deterministic and	Twelve catchments in	_
	probabilistic methods,	the Netherlands	
	namely Sparse,		
	DenseRotation, S-		
	PROG, and STEPS,		
	implemented within		
	Rainymotion (Ayzel et		
	al. 2019) and		
	pySTEPS (Pulkkinen		
	et al. 2019)		

Reinoso-Rondinel et al. (2022)	S-PROG (deterministic; Seed 2003)	Germany	
Berenguer et al. (2005)	S-PROG (deterministic; Seed 2003), Lagrangian advection and Eulerian persistence (deterministic)	Barcelona, Spain	DiCHiTop (distributed)
Šálek et al. (2006)	COTREC (deterministic; Li et al. 1995)	Czech Republic	HYDROG (distributed)
Vivoni et al. (2006)	STNM algorithm (deterministic; Wolfson et al. 1999)	Midwestern United States	tRIBS (physically- based, distributed)
Xuan et al. (2014)	STEPS (probabilistic; Bowler et al. 2006)	One catchment in the United Kingdom	PDM (lumped)
Heuvelink et al. (2020)	Lagrangian persistence/COTREC (deterministic; Li et al. 1995) and SBMcast (probabilistic; Berenguer et al. 2011)	Three catchments in the Netherlands	WALRUS (lumped)
Lovat et al. (2022)	AROME-NWC (deterministic, NWP- based; Auger et al. 2015) and PIAF (combination of radar nowcasts and NWP; Moisselin et al. 2019)	Nineteen catchments in south-eastern France	ISBA-TOP (distributed)
Imhoff et al (2022)	Four deterministic and probabilistic methods, namely Sparse, DenseRotation, S-PROG, and STEPS, implemented within Rainymotion (Ayzel et al. 2019) and pySTEPS (Pulkkinen et al. 2019)	Twelve catchments in the Netherlands	SOBEK (semi- distributed) and WALRUS (lumped)

Table 1. Summary of applications using deterministic and probabilistic precipitation nowcasting methods with and without hydrological evaluation.

Despite these findings, previous studies did not focus on the evaluation methodology of the nowcasting techniques. Namely, all of the listed studies (except Imhoff et al. 2022) adopted a single modeling approach (i.e., either lumped or distributed, conceptual or physically-based), which did not allow for considering how the choice of the hydrological model structure impacted the evaluation of the nowcasting techniques (such as done by Poméon et al., 2020). In addition, the impact of the benchmark nowcasting model (such as zero-precipitation nowcasts or hydrological persistence) on the forecasting skill remains

115	poorly investigated while it can have significant impact on the estimated added value of QPN
116	(Pappenberger et al. 2015b).

To tackle these gaps, we evaluated one probabilistic (STEPS) and two deterministic nowcasting techniques (advection-based and S-PROG) by measuring their ability in forecasting simulated hydrographs with QPE. Our study focuses on the disastrous mid-July 2021 events in seven catchments located in western Germany. These events caused more than 220 deaths and costed up to €32.05 billion in total losses in Germany alone, making them one of the most severe natural disasters caused by heavy rain and flooding in Germany (Mohr et al. 2023). We adopted a novel multi-modeling approach by evaluating QPN as inputs to a conceptual, lumped model (GR4H) and to a physically-based, 3D-distributed model (ParFlowCLM). Thus, the aim of this study is to investigate whether a more detailed representation of hydrological processes leads to a better discrimination of QPN compared to a simpler, lumped one. Moreover, we checked whether different choices of skill evaluation and benchmarks impact the estimation of the added value of the nowcasting techniques.

This paper is organized as follows. Section 2 presents the case study, the catchment set, and the QPE product used to produce the QPN. Section 3 introduces the tested nowcasting techniques, the hydrological models and the evaluation framework, while Sections 4 and 5 comment and discuss the results. Finally, Section 6 concludes our study.

2. Catchment set and QPE product

In July 2021, sustained stratiform rain connected to a cut-off low pressure system (Junghänel et al. 2021) led to record-breaking precipitation amounts and disastrous floods (Kreienkamp et al. 2021; Mohr et al. 2023), especially over relatively high altitudes at the Eifel range on the left bank of the Rhine river and the Bergisches Land on the right bank (Figs. 1 and 2). On 14 July 2021, observed total precipitation sums exceeded 160 mm at some rain gauges (Fig. 2c), which is equivalent to two to three months of accumulated precipitation based on the annual averages (i.e., by dividing 160 mm by the annual averages listed in Table 2). Since rain gauges do not provide a detailed description of the spatial variability of precipitation, measurements from four polarimetric C-band radars (located at Essen, Flechtdorf, Neuheilenbach, and Offenthal; Fig. 2a), operated by the German Weather Service (DWD), were exploited to derive a gridded QPE product for the 14 July 2021 (Fig. 2b) with 1-km horizontal resolution and 5-min temporal resolution. This hybrid product combines

precipitation estimates derived from specific attenuation at vertical polarization A_V , $R(A_V)$, with retrievals of specific differential phase K_{DP} for horizontal reflectivity rates Z_h higher than 40 dBZ, $R(K_{DP})$. This product clearly outperformed retrievals based on horizontal reflectivity alone (Chen et al. 2021; Saadi et al. 2023). The hybrid QPE product, referred to as RAVKDP in the following, served as input for QPN algorithms.

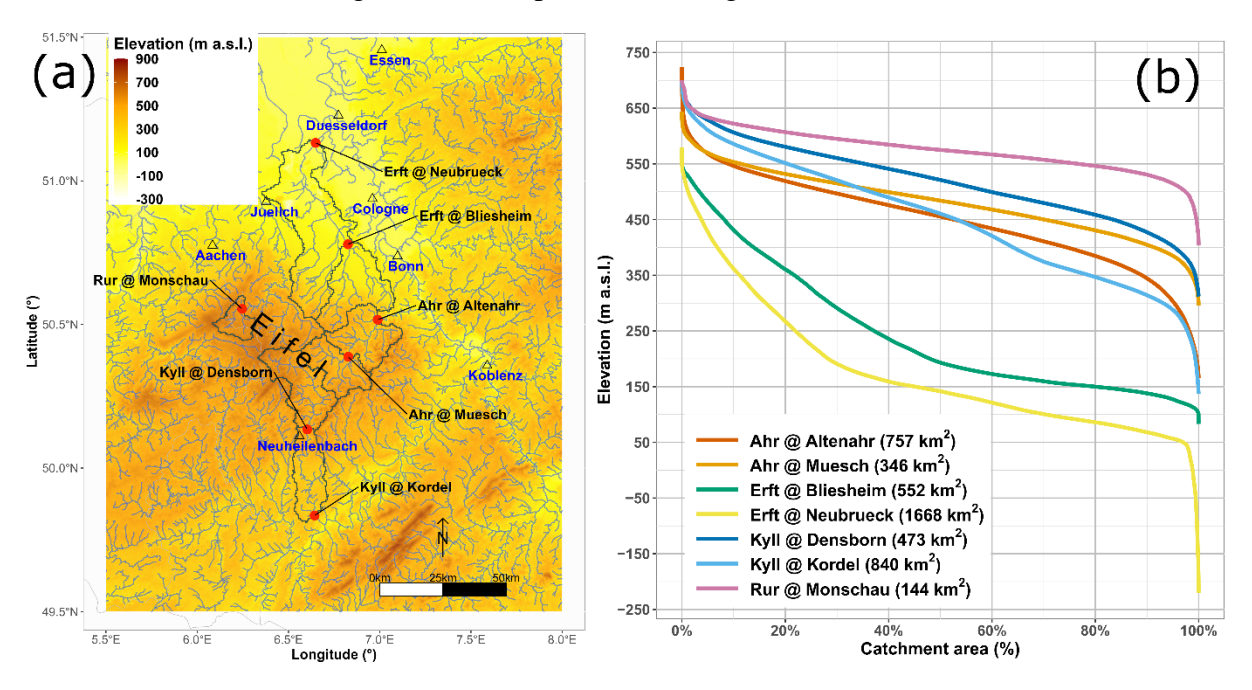


Fig. 1. (a) Location, topography and hydrographic network of study catchments, where contours indicate the catchment polygons, and (b) hypsometric curves of the catchment set. Negative elevations are due to the existence of open-pit mines in the region.

157

158 159

160

161

162

163

164 165

166

167

168

169

170

171

172

173

174

175

176

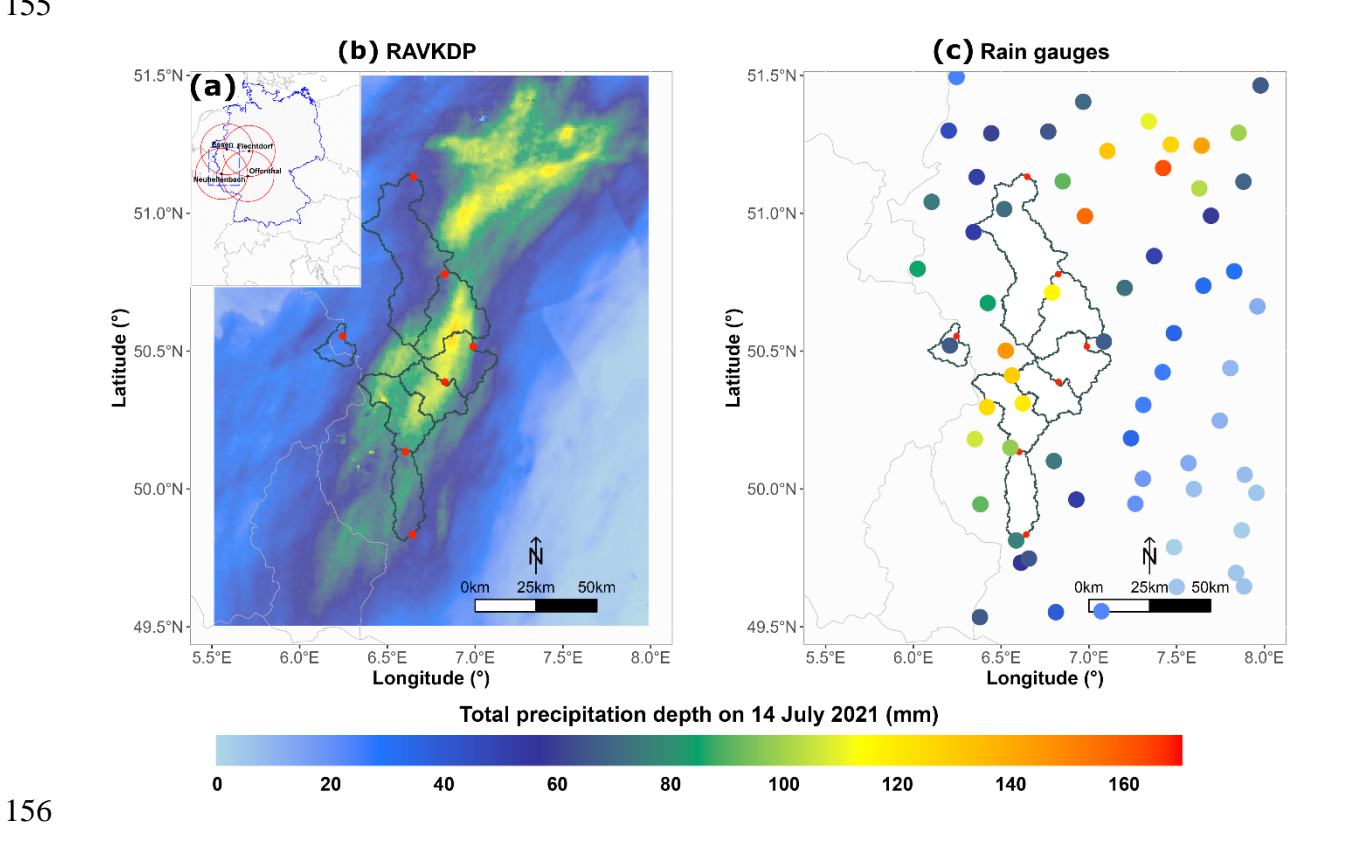


Fig. 2. (a) Location of the four C-band radars (Essen, Flechtdorf, Neuheilenbach, and Offenthal) operated by the German Weather Service (DWD) and used to derive the QPE product RAVKDP. (b) Total precipitation amounts on 14 July 2021 (from 0000 UTC 14 July 2021 to 0000 UTC 15 July 2021) estimated from the radar-based QPE RAVKDP and (c) from 63 rain gauges. For the 63 rain gauges, the ratio of total precipitation from RAVKDP to that from the rain gauge varied between 0.27 and 3.00, with a median value of 0.72. The light grey contours indicate the borders with the neighboring countries (The Netherlands, Belgium, Luxembourg, and France).

To hydrologically evaluate the benefits of QPN, we selected a set of seven catchments located in western Germany that drain parts of the Eifel mountain range (Fig. 1a), characterized by a rolling plateau at elevations up to 750 m a.s.l. (Fig. 1b). These catchments have areas ranging between 140 and 1670 km² (Table 2). Three of the seven catchments are located in the federal state of North Rhine-Westphalia and are drained by the Erft and the Rur rivers. The remaining four catchments are located in the federal state of Rhineland-Palatinate and are drained by the Ahr and the Kyll rivers. The region is characterized by a temperate climate under maritime influence, which is reflected by the range of the average annual precipitation amounts (710 to 1070 mm/yr) and the values of the aridity index as defined by the United Nations Environment Programme (1.13 to 1.92; UNEP 1992). The land cover of the catchments is mainly occupied by forest and agricultural areas according to the CORINE Land Cover database of 2018 (Langanke et al. 2016). Soils are dominated by sand (34%-

41%) and silt contents (29%-38%; Panagos, 2006). To estimate total precipitation amounts on 14 July 2021 at the catchment scale, we applied the Thiessen polygon method on measurements from rain gauges and on RAVKDP. Estimated precipitation amounts from rain gauges varied between 66 and 121 mm across our catchment set (Table 2), reflecting the severity of the event and its variability from one catchment to another. Based on RAVKDP, obtained estimates totaled only 34 mm to 90 mm (Table 2), indicating an underestimation with respect to estimated amounts from rain gauges. This underestimation is partly attributed to collision-coalescence processes that took place close to the surface, i.e. below the heights monitored by the radars (Saadi et al. 2023; Chen et al. 2022).

River ^a	Area (km²	Average precipitation (mm/yr)	Aridity index ^b (-)	Average discharge (mm/yr)	Artificial ^c (%)	Agricultural ^c (%)	Forest ^c (%)	Total precipitation amount on 14 July 2021 (mm) from RAVKDP/rain gauges (number of rain gauges)
Erft at Neubrueck	1668	740 (2006- 2021)	1.16	180 (2000- 2020)	17.7	64.3	17.8	66/99 (13)
Kyll at Kordel	840	830 (2006- 2021)	1.41	370 (1967- 2021)	5.4	51.9	42.7	80/103 (10)
Ahr at Altenahr	757	750 (2006- 2021)	1.27	280 (1945- 2021)	3.5	39.5	57	89/108 (7)
Erft at Bliesheim	552	710 (2006- 2021)	1.13	130 (2000- 2020)	12.6	59.1	28.2	88/108 (7)
Kyll at Densborn	473	890 (2006- 2021)	1.54	450 (1972- 2021)	4	47.7	48.2	87/115 (7)

Ahr at Muesch	346	790 (2006- 2021)	1.34	280 (1972- 2021)	4	52.9	43.1	90/121 (6)
Rur at Monschau	144	1070 (2006- 2021)	1.92	760 (2000- 2021)	6.1	25.4	62.9	34/66 (1)

^aAll catchments contain at least one reservoir (lake or dam) according to the database at https://dewiki.de/Lexikon/Liste von Talsperren in Deutschland (in German, last access: 14 April 2023).

- Table 2. Summary of catchment characteristics. Catchment-average, total precipitation
- amount on 14 July 2021 (from 0000 UTC 14 July 2021 to 0000 UTC 15 July 2021) are
- extracted from RAVKDP, the radar-based QPE product, and from rain gauges using Thiessen
- polygons. In the far-right column, the total number of rain gauges used for the 14 July 2021
- 190 for each catchment is provided between brackets.

3. Evaluation of the added value of QPN

192 a. Tested nowcasting techniques

191

196

197

198

199

200

201

202

203

204

- Based on the QPE product RAVKDP, we computed 3-h long QPN with 1-km spatial and
- 5-min temporal resolution. In this study, three nowcasting strategies following Reinoso-
- 195 Rondinel et al. (2022) have been applied:
 - 1. The deterministic method based on Lagrangian persistence (advection-based) assumes a constant precipitation field (i.e., with no growth or decay) advected using a static motion field. First, the motion field was estimated from the RAVKDP product using the optimal-flow method DARTS (Ruzanski et al. 2011). Then, the latest observed precipitation field is advected along the estimated motion trajectories for the next three hours using a semi-Lagrangian backward scheme (Germann and Zawadzki 2002).
 - 2. The deterministic method S-PROG (Spectral Prognosis; Seed, 2003) assumes that the spatial scale of precipitation features is on par with its lifetime and thus its predictability. This means that larger precipitation features tend to last longer and can

^bThe aridity index was computed as the ratio of average annual precipitation to average annual atmospheric evaporative demand, which we expressed as the average annual potential evapotranspiration (UNEP 1992). Potential evapotranspiration was computed using a temperature-based formula (Oudin et al. 2005).

[&]quot;These metrics were computed based on the CORINE Land Cover classification of the Copernicus Land Monitoring Service (Langanke et al. 2016). They correspond to the proportion of the catchment that is occupied by the classes belonging to (1) "Artificial Surfaces" for Artificial, (2) "Agricultural areas" for Agricultural, and (3) "Forest and seminatural areas" for Forest. See https://land.copernicus.eu/user-corner/technical-library/corine-land-cover-nomenclature-guidelines/html (last access: 14 April 2023).

be predicted with larger lead times. First, the precipitation field is decomposed into a
multiplicative cascade of spatial scales. Second, an autoregressive model (AR) is used
to model and forecast the temporal evolution and to advect each cascade level.
Finally, the nowcasted field is computed as the aggregation of the advected cascade
levels. This leads to a smoothing of the precipitation field as the small-scale, high-
frequency features tend to vanish with time according to the AR model. Compared
with Seed (2003), we kept the order of the AR model at 1 instead of 2, and we fixed
the number of levels of the multiplicative cascade at 6, resulting in the following
spatial scales of 900, 56, 20, 7, 3, and 1 km. Moreover, we used the precipitation field
instead of the reflectivity field. Since the precipitation field does not follow a
Gaussian distribution, the above processes were applied to the log-transformed values
of precipitation, which we assumed to have a near-Gaussian distribution. After
extrapolation, an inverse transformation was applied to the nowcasted precipitation
field. These choices follow the study by Reinoso-Rondinel et al. (2022).

- 3. The probabilistic method STEPS (Short-Term Ensemble Prediction System; Bowler et al., 2006) builds on S-PROG by adding stochastic perturbations to account for the uncertainties in the estimated motion field and the evolution of the precipitation cells. More precisely, each cascade level is perturbed by Gaussian white noise that is correlated with the spatial properties of the last observed precipitation field (Seed et al. 2013), which leads to an ensemble of QPN. In our study, we considered an ensemble of 20 members.
- For each QPN method, we generated 3-h long time series of nowcasted precipitation each 5 min (i.e., at 0000 UTC, 0105 UTC, 0110 UTC 14 July 2021, etc.) with a temporal resolution of 5 min. Since we chose to feed these QPN to hourly hydrological models, we kept only QPN that were issued at round hours (i.e., at 0100 UTC, at 0200 UTC, ..., and at 1800 UTC 14 July 2021) and discarded the remaining ones. In addition, we aggregated the 5-min QPN time series to obtain hourly accumulations of precipitations.

b. Hydrological models

We analyzed the impact of the hydrological model on the evaluation of QPN by selecting two contrasting modeling approaches, for which the implementation is described in Table 3. As a physically-based, distributed model, we used ParFlow with its internal land surface module CLM (Common Land Model), hereafter ParFlowCLM (Kollet and Maxwell 2006;

Kuffour et al. 2020; Maxwell 2013). CLM estimates the actual evapotranspiration, infiltration, and net precipitation (i.e., the part that gives rise to runoff) by resolving the energy budget at the land surface and the water exchange at the interface between the atmosphere, the land, and the soil. ParFlow solves the 3D Richards' equation for variably saturated subsurface and groundwater flow and the kinematic wave equation for the overland flow routing. These two equations are coupled at the land surface by estimating the boundary fluxes for the kinematic wave model from Richards' equation, and vice versa. Thanks to this coupling, the model represents a variety of runoff processes (Hortonian vs. Dunne runoff) as well as the re-infiltration and exfiltration processes along the hydraulic pathway. We implemented ParFlowCLM at a resolution of 611 m with 15 vertical layers down to 60 m below the surface (Belleflamme et al. 2023). It was forced with gridded weather inputs over a spin-up period starting from 2007, with only one parameter set for each catchment based on landscape properties, as detailed in Table 3.

As a conceptual, lumped model, we chose GR4H (Ficchì et al. 2019). This model estimates net precipitation and actual evapotranspiration using a soil-moisture accounting reservoir. The net precipitation gives rise to runoff through two routing branches. The quick flow branch transfers 10% of net precipitation via a unit hydrograph, while the slow flow branch transfers the remaining 90% via a unit hydrograph and a nonlinear reservoir. Over both branches, an exchange between surface flow and groundwater is enabled. GR4H uses catchment-average weather inputs to simulate the discharge at the catchment outlet. Model parameters were estimated using historical discharge measurements over the period 2007-2021, with a spin-up over the year 2006 to limit the effect of model initialization on calibration. We tested several choices of calibration combining the sub-period of calibration, the cost function, and the weights attributed to discharge measurements to emphasize high values, yielding 12 optimal parameter sets for each catchment (Saadi et al. 2023).

Model	Spatial and	Parameter estimation	Hydroclimatic data
	temporal		
	resolution		

ParFlowCLM

~611 m horizontal resolution with a geometrically varying vertical resolution, hourly Topography: ASTER^a DEM^b (Abrams et al. 2020;

https://lpdaac.usgs.gov/products/astgtmv003) combined with MERIT^c Hydro (Yamazaki et al. 2019).

Soil and geology: SoilGrids250m (Hengl et al. 2017), reclassified into 12 USDA^d texture types, and IHME1500^e (Duscher et al. 2015) for the typology below the depth to bedrock; ROSETTA model (Schaap et al. 2001) to obtain hydraulic parameters (hydraulic conductivity, residual and saturated water content, and van Genuchten parameters) depending on soil types.

Land cover: CORINE^f Land Cover database of the CLMS^g for the year 2018 (Langanke et al. 2016; https://land.copernicus.eu/pan-european/corine-land-cover/clc2018, last access: 12 March 2020), reclassified into 18 IGBP^h categories. A uniform Manning's coefficient at 0.2 s·m^{-1/3} (Schalge et al. 2019) was used for the whole domain.

Only one parameter set for each catchment (Belleflamme et al. 2023).

Precipitation: RADOLANⁱ of the DWD^j (Winterrath et al. 2018), which is a Germany-wide, radarbased near-real time precipitation product available at 1-km resolution and hourly time steps obtained using relationships between horizontal reflectivity and precipitation rates, and then adjusted to rain gauges (i.e., RADOLAN-RW, https://opendata.dwd.de/, last access 14 April 2023). RAVKDP was used for precipitation on 14 July 2021 (Chen et al. 2021).

2-m air temperature, surface pressure, downward solar and thermal radiation, specific humidity, and eastward and northward components of the 10-m wind: ERA5-Land dataset (Muñoz-Sabater et al. 2021), available at 9-km resolution.

GR4H	Lumped, hourly	Four catchment-scale parameters representing the maximum retention capacity of the soil, the exchange between surface water and groundwater, the surface flow dynamics and the baseflow dynamics. These parameters are calibrated on historical discharge measurements using a gradient-descent based algorithm (Coron et al. 2017; Edijatno et al. 1999). 12 optimal sets of 4 parameters for each catchment (Saadi et al. 2023).	Catchment-averaged precipitation: RADOLANi of the DWDi (Winterrath et al. 2018), available at 1-km and hourly resolutions, estimated based on horizontal reflectivity and adjusted to rain gauges (i.e., RADOLAN-RW, https://opendata.dwd.de/, last access 14 April 2023). RAVKDP was used for precipitation on 14 July 2021 (Chen et al. 2021). Thiessen polygons were used to estimate the catchment-average precipitation at each hour. Catchment-averaged potential evapotranspiration: obtained from catchment-average, 2-m air temperature using a temperature-based formula (Oudin et al. 2005). Discharge: used for model calibration, available at daily resolution (https://www.elwasweb.nrw.de; https://wasserportal.rlp-umwelt.de, last access: 20
			September 2021).
^a A dyanced	Spacehorne Thern	nal Emission and Reflection Radiometer: bDigital	l elevation model: ^c Multi-Error-

^aAdvanced Spaceborne Thermal Emission and Reflection Radiometer; ^bDigital elevation model; ^cMulti-Error-Removed Improved Terrain; ^dUnited States Department of Agriculture; ^eInternational Hydrogeological Map of Europe at the scale of 1:1500000; ^fCoordination of Information on the Environment; ^gCopernicus Land Monitoring Service; ^hInternational Geosphere-Biosphere Programme; ⁱRadar-Online-Aneichung; ^jDeutscher Wetterdienst (German Weather Service)

- Table 3. Details of ParFlowCLM and GR4H implementation: resolution, parameter estimation, and sources of hydroclimatic data needed for each model.
- 265 c. Comparison and evaluation framework of QPN

266

267

268

269

270

Following Berenguer et al. (2005), we evaluated the skill of QPN on two levels. On the first level, we analyzed how QPN succeeded in matching QPE for each lead time, first at the grid-cell scale, then at the catchment scale by averaging the precipitation fields using the catchment polygon. At the grid-cell scale, we adopted the mean absolute error MAE (mm/h) and the root-mean-square error RMSE (mm/h) as evaluation metrics, expressed as:

MAE (L) =
$$\frac{1}{N_t \cdot N_c} \sum_{i=1}^{N_c} \sum_{t=1}^{N_t} |\widehat{P_{t+L|t}}(i) - P_{t+L}(i)|$$
 (1)

RMSE (L) =
$$\sqrt{\frac{1}{N_t \cdot N_c} \sum_{i=1}^{N_c} \sum_{t=1}^{N_t} (\widehat{P_{t+L|t}}(i) - P_{t+L}(i))^2}$$
 (2)

271

272

273

274

275

276

277

278

279

280

281

282

283

284

285

286

287

288

289

290

291

292

where N_t is the number of initialization time steps (i.e., hours or 5-min time steps between 0100 UTC 14 July 2021 and 1800 UTC 14 July 2021), N_c is the number of grid cells, L is the lead time, $\widehat{P_{t+L|t}}(i)$ is the QPN intensity for the time step t+L issued at time step t for the grid cell i, and $P_{t+L}(i)$ is the QPE intensity at time step t+L for the grid cell i. Both RMSE (mm/h) and MAE (mm/h) vary between 0 (perfect match) and $+\infty$. Note that for the computation of the spatial average of MAE and RMSE, we excluded the grid cells for which the total precipitation amount on 14 July 2021 (according to RAVKDP) was equal to zero. By this choice, we aimed at limiting the number of grid cells for which the errors are equal or very close to zero, the inclusion of which would artificially decrease the two accuracy measures. At the catchment scale, we first averaged the precipitation time series using the catchment polygon, then we computed the MAE between the resulting catchment-scale QPE time series and catchment-scale QPN time series. For the probabilistic STEPS method, since each member served as input to the hydrological models, both MAE and RMSE scores were estimated for each of the 20 members, then for a deterministic nowcast STEPS-m taken as the ensemble mean at each grid cell and at each time step. Following the approach by Foresti et al. (2016), we also aimed at analyzing the spread of the ensemble with respect to the errors of the deterministic forecast (i.e., S-PROG or STEPS-m) in order to qualify whether the ensemble was under-dispersive (i.e., underestimating the uncertainty in the evolution of the precipitation field) or overdispersive (i.e., overestimating the uncertainty in the evolution of the precipitation field; see Foresti et al. 2016). To this aim, we estimated the spread of the ensemble at the grid-cell scale at each lead time using the following equation (Foresti et al. 2015):

spread (L) =
$$\sqrt{\frac{1}{N_t \cdot N_c} \sum_{i=1}^{N_c} \sum_{t=1}^{N_t} \frac{1}{M-1} \sum_{m=1}^{M} \left(\widehat{P_{t+L|t}}(i, m) - \overline{\widehat{P_{t+L|t}}}(i) \right)^2}$$
 (3)

where M = 20 is the total number of members, $\widehat{P_{t+L|t}}(i, m)$ is the QPN intensity for the time step t + L issued at time step t for the grid cell i by the STEPS member m, and $\widehat{\overline{P_{t+L|t}}}(i)$ is the intensity of the STEPS ensemble mean nowcast at time step t + L issued at time step t for the grid cell i. Ideally, the spread should be of the same order of variability of the QPE around the ensemble mean, measured in our case by the RMSE of the ensemble mean nowcast STEPS-m. When the spread is higher than this RMSE, the ensemble is over-dispersive, otherwise the ensemble is under-dispersive (Foresti et al. 2016).

On the second level, QPN were used to extend the precipitation input to the hydrological models. First, both models were run prior to 0100 UTC 14 July 2021 with the version of RADOLAN that was adjusted to rain gauges (i.e., RADOLAN-RW; Winterrath et al. 2018) as input precipitation (see Table 3). These runs started from January 2021 for ParFlowCLM and from 2007 for GR4H. Starting from 0100 UTC 14 July 2021, the QPE product RAVKDP was used instead of RADOLAN for our study region. At each initialization hour (e.g., 0100 UTC 14 July 2021), the QPE was replaced by the 3-h QPN (e.g., at 0200 UTC, 0300 UTC and 0400 UTC) followed by zero precipitation (e.g., from 0500 UTC onward). Then, the resulting forecasted hydrographs were compared to the simulated hydrograph with the QPE product RAVKDP as input for 14 July 2021 and RADOLAN as input for the remaining days (i.e., the hindcasted hydrograph).

In a first step, we evaluated the quality of the hydrological forecasts obtained by the use of QPN and the benchmarks using the Nash-Sutcliffe Efficiency score (NSE, Nash and Sutcliffe 1970), computed as:

NSE (L) =
$$1 - \frac{\sum_{t=1}^{N_t} (Q_{t+L} - \widehat{Q_{t+L}})^2}{\sum_{t=1}^{N_t} (Q_{t+L} - \overline{Q_{t+L}})^2}$$
 (4)

where $\widehat{Q_{t+L|t}}$ is the forecasted discharge values at the time step t+L initialized at the time step t, Q_{t+L} the hindcasted discharge values (i.e., simulated hydrographs using QPE) at time step t+L and $\overline{Q_{t+L}}$ their average. NSE varies between $-\infty$ and 1, the latter being the ideal value. As the lead time increases, NSE is expected to decrease. Fig. 8 of Berenguer et al.

- 318 (2005) and Fig. 2 of Heuvelink et al. (2020) illustrate the application of this evaluation
- 319 method.
- The added value of each QPN can be estimated by comparison with a
- benchmark/reference option (Pappenberger et al. 2015b). To measure this added value, we
- 322 computed the gain in lead time defined as (Berenguer et al. 2005):

Gain in lead time =
$$L_{QPN}(NSE_{th}) - L_{Ref}(NSE_{th})$$
 (5)

- where $L_{OPN}(NSE_{th})$ is the lead time at which the obtained NSE with the QPN as input to the
- hydrological model equals NSE_{th} for the first time, and $L_{Ref}(NSE_{th})$ is the lead time at which
- 325 the obtained NSE with the benchmark Ref equals NSE_{th} for the first time. Following
- Heuvelink et al. (2020), we adopted a threshold of $NSE_{th} = 0.9$. To analyze the impact of
- 327 this threshold, we computed the gain for an additional threshold of $NSE_{th} = 0.5$.
- In a second step, we applied the average of the Continuous Ranked Probability Score
- 329 CRPS (Hersbach 2000), expressed for each lead time L as:

CRPS (L) =
$$\frac{1}{N_t} \sum_{t=1}^{N_t} \int_0^{+\infty} \left(F_{\widehat{Q_{t+L}|t}}(x) - \mathbb{1}\{Q_{t+L} \le x\} \right)^2 dx$$
 (6)

- 330 where $F_{\widehat{Q_{t+L}|t}}$ is the cumulative distribution function of the forecasted discharge values $\widehat{Q_{t+L}}$
- initialized at the time step t for the time step t + L, and Q_{t+L} is the value at time step t + L of
- 332 the simulated hydrograph using QPE (i.e., the hindcasted hydrograph). $\mathbb{1}\{y \le x\}$ is the
- Heaviside step function that equals 1 if $y \le x$ and 0 otherwise. CRPS was chosen because it
- helps undistinguishably evaluate both the probabilistic and the deterministic nowcasting
- methods. For a deterministic forecast, it is equivalent to MAE.
- To evaluate the added value of the QPN methods with respect to a benchmark, a skill
- score based on the CRPS was computed as follows (Chen et al. 2017):

$$Skill_{CRPS,Ref} = \frac{CRPS(Ref)}{CRPS(QPN) + CRPS(Ref)}$$
(7)

- which is a bounded (between 0 and 1) and a scale-independent metric. A skill higher than 0.5
- indicates that the forecasts obtained with QPN are better than the ones obtained with the
- benchmark (i.e., CRPS(QPN) < CRPS(Ref)), and vice versa.
- To investigate the effect of the benchmark choice on the evaluation of QPN, we evaluated
- 342 the skill of QPN with respect to: (1) a hydrological persistence model (Berthet et al. 2009)

that forecasts the future discharge to be constant and equal to the hindcasted discharge at the hour of initialization (Skill_{CRPS, O}), and (2) a forecasted hydrograph using zero precipitation nowcasts (ZNC; Heuvelink et al. 2020; Berenguer et al. 2005) as QPN (Skill_{CRPS, ZNC}). The latter is costlier than the former because it involves running the hydrological model for the ZNC. Finally, for the CRPS-based skill in Eq. 7, we retrieved the lead time up to which QPN is considered to be "useful" with respect to the benchmark using two skill thresholds: the theoretical one at 0.5, and a more demanding one $(2/3 \approx 0.67)$, which is equivalent to CRPS(QPN) $< \frac{1}{2}$ CRPS(Ref)).

To qualitatively analyze the effect of catchment properties on the added value of QPN with respect to the benchmark, the gains in lead time based on NSE (Eq. 4) and based on the skills (Eq. 7) were ranked first with respect to catchment area, and second with respect to the Gravelius index of the catchment, defined as (Bendjoudi and Hubert 2002):

$$K = \frac{P}{2\sqrt{\pi A}} \tag{8}$$

where P is the perimeter of the catchment polygon (in km) and A the catchment area (in km²). Catchments with lower K tend to have compact or circular shapes, which would generally result in flashier hydrological responses for a given precipitation event covering the whole catchment.

4. Results

a. Evaluation of QPN with respect to QPE

Aggregating the QPN time series to the hourly time step reduced the differences between the three methods and modified their ranking, as can be seen in Fig. 3. At 5-min resolution (Figs. 3a and 3b), QPN obtained by advection and STEPS had similar MAE and RMSE scores over the domain along the lead times. As the lead time increased, S-PROG clearly outperformed the other two QPN methods. At 1-h resolution (Figs. 3c and 3d), the three methods obtained lower MAE and RMSE values compared with the 5-min resolution, S-PROG preserved its ranking with respect to advection and STEPS, whereas advection slightly outperformed the STEPS ensemble, suggesting that changing the accumulation window can modify the ranking of the QPN methods. For both time resolutions, the STEPS ensemble mean STEPS-m outperformed all the other members for all time steps, suggesting that the stochastic perturbations of the S-PROG method (materialized by STEPS members) got

penalized for this event. Finally, there were very small differences between the different STEPS members in terms of MAE and RMSE (hardly visible in Fig. 3), which is somewhat expected from averaging the errors in space (over the domain) and time (across the initialization time steps) for members generated randomly and independently for each initialization. The small spread of STEPS members compared with the RMSE of the ensemble mean STEPS-m or the RMSE of the deterministic S-PROG method suggests that the ensemble nowcasts were under-dispersive (Foresti et al. 2016), i.e. that they underestimated the uncertainty in the nowcasted precipitation field for this event.

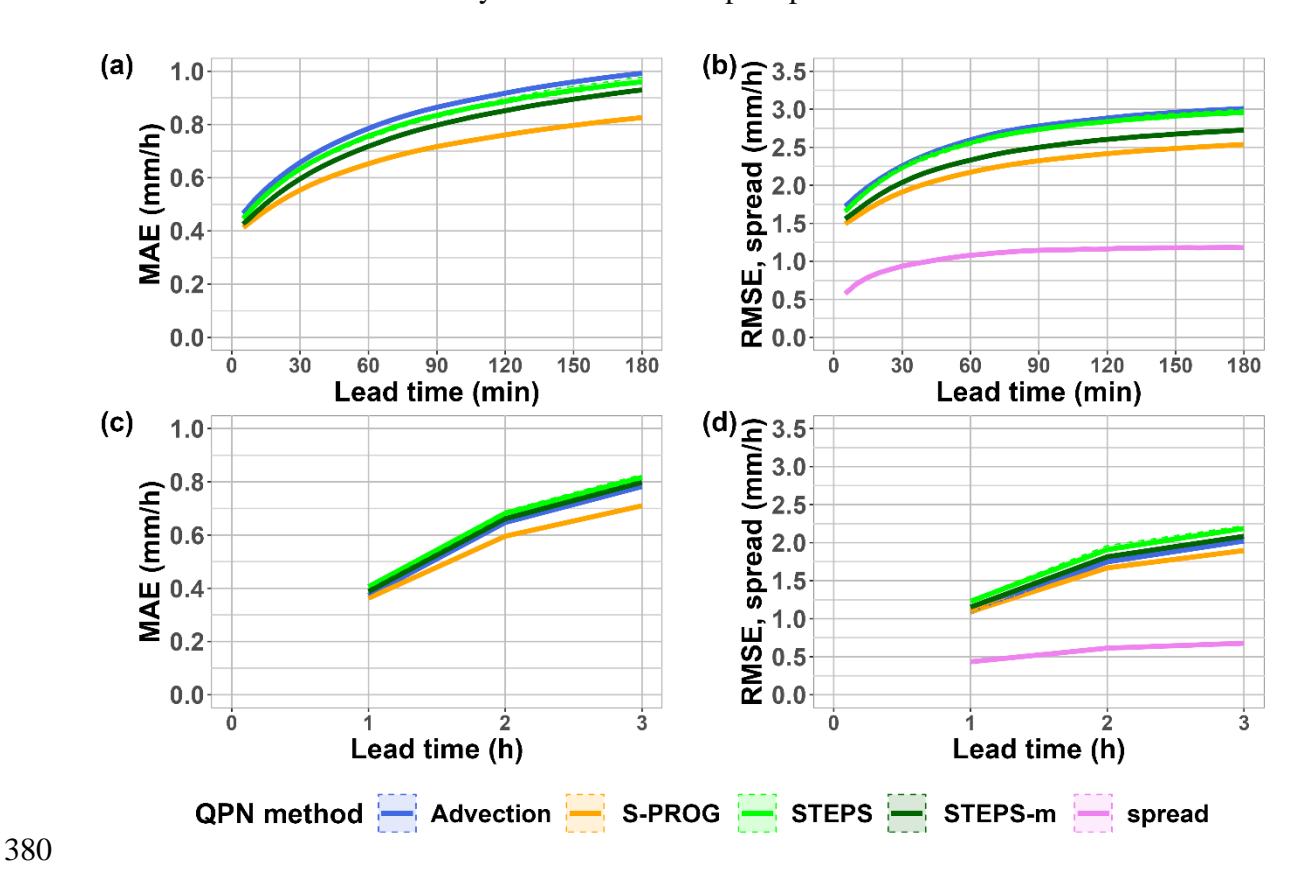


Fig. 3. Evolution of the spatial average of mean absolute errors (MAE) and root-mean-square errors (RMSE) of QPN with respect to precipitation rates from the QPE product RAVKDP for different lead times at 5-min resolution updated each 5 min for (a) and (b), and at 1-h resolution updated each hour for (c) and (d). In (b) and (d), "spread" indicates the spread of the STEPS ensemble (Eq. 3). STEPS-m indicates the ensemble mean, i.e., the nowcast made by taking the average of the nowcasted depths from the 20 STEPS members at each grid cell and each time step. The spatial average was computed on all domain grid cells except the ones with zero-precipitation amounts on 14 July 2021 according to the QPE product RAVKDP. The ensemble of MAE and RMSE errors for the STEPS method is hardly visible due to very small differences between the members.

At the hourly time step, the three QPN methods showed comparable performances in reproducing the observed precipitation at the grid-cell-scale, with a slightly higher

performance for S-PROG, as shown in Fig. 4. The spatial pattern of MAE followed that of the precipitation sums for the event (Fig. 2b), with a slight shift for the part of the event cell located over the catchment set to the south-west. Unsurprisingly, the errors were minimal for the shortest lead time (i.e., 1 h) and increased with increasing lead time. For the 1-h lead time, domain-average MAE values were around 0.36-0.37 mm/h for the advection and S-PROG methods, whereas they reached 0.39 mm/h on average for STEPS members, indicating a slightly deteriorated accuracy for the probabilistic QPN. For the 3-h lead time, these errors more than doubled and reached 0.77 mm/h for advection, 0.7 mm/h for S-PROG, and 0.79 mm/h on average for STEPS, indicating a better performance of the S-PROG method over the domain.

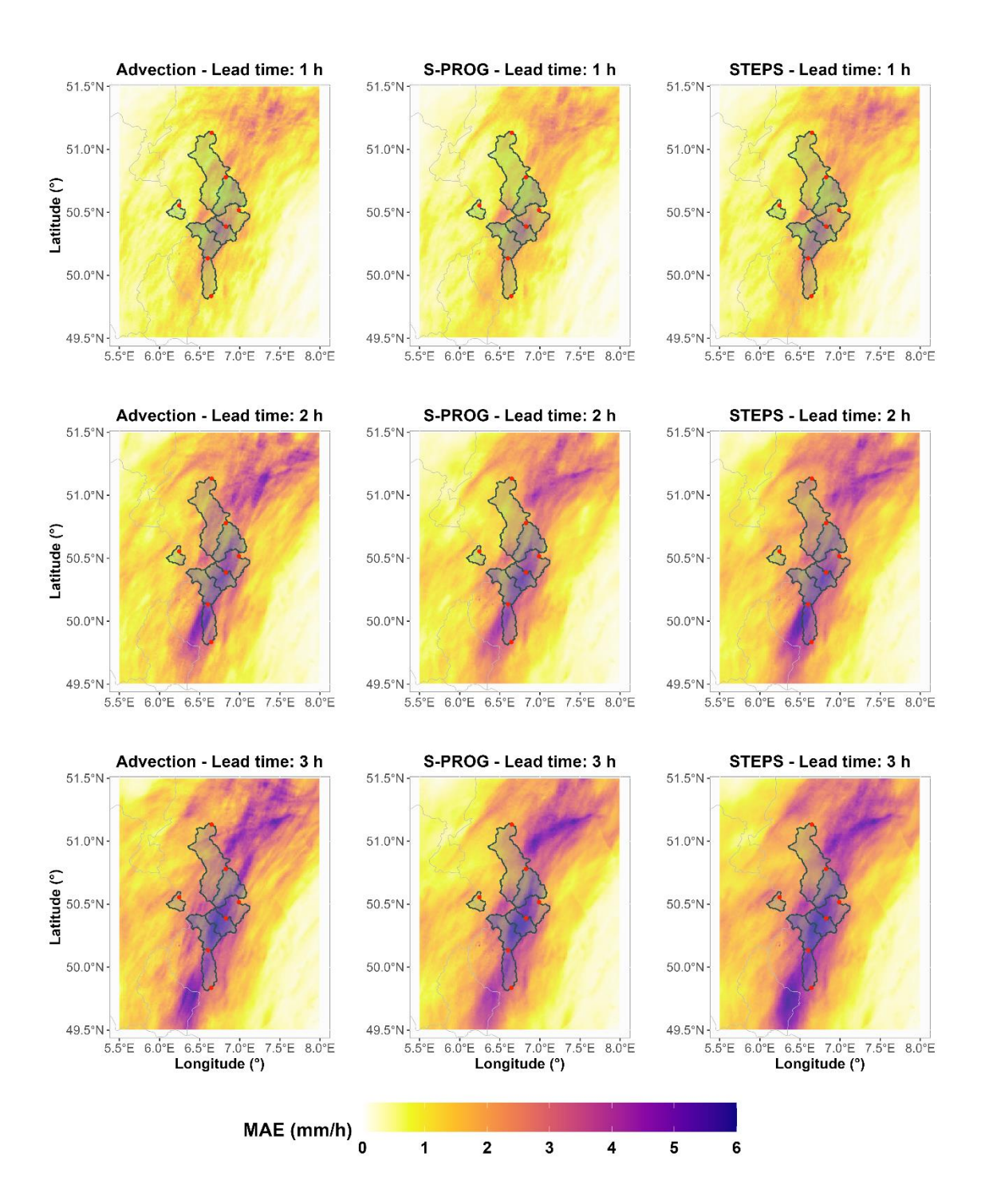


Fig. 4. Mean absolute errors (MAE) of QPN obtained using advection (left column), S-PROG (middle column) and STEPS for the 1-h lead time (top row), 2-h lead time (middle row) and 3-h lead time. MAE values were computed with respect to observed precipitation rates from RAVKDP. For STEPS, the median errors over the 20 members is shown.

At the catchment scale, the advection method obtained slightly better results than S-PROG and STEPS, as shown in Fig. 5. The change in the ranking of the QPN methods with respect to Fig. 3 may be explained by the catchment-scale aggregation of the precipitation fields prior to the computation of the errors, or the fact that the catchments do not cover the whole

domain on which MAE values of Fig. 3 were computed (see Fig. 2b and Fig. 4). Moreover,
advection does not change QPE intensities across the lead times, whereas S-PROG filters the
observed QPE field, leading to smoother QPN field and to an underestimation of precipitation
for persistent and heavy events. This results in advection mimicking better the QPE than S-
PROG, especially over our catchment set where the July 2021 event was persistent and
heavy. Overall, QPN had better success in reproducing the average precipitation for the
catchments drained by the Rur at Monschau and the Erft than for the catchments drained by
the Kyll and the Ahr. The variability in the ensemble errors of STEPS increased with
increasing lead time. In addition, the errors of the STEPS method bracketed those of the two
deterministic methods except for some cases where the advection showed a lower error than
the whole STEPS ensemble. The evolution of the errors does not indicate a dependency on
catchment size, although the largest catchment (Erft at Neubrueck) showed lower MAE
errors for a lead time of 3 h. The variability of errors across the catchments reflects the effect
of their location with respect to the precipitation field.

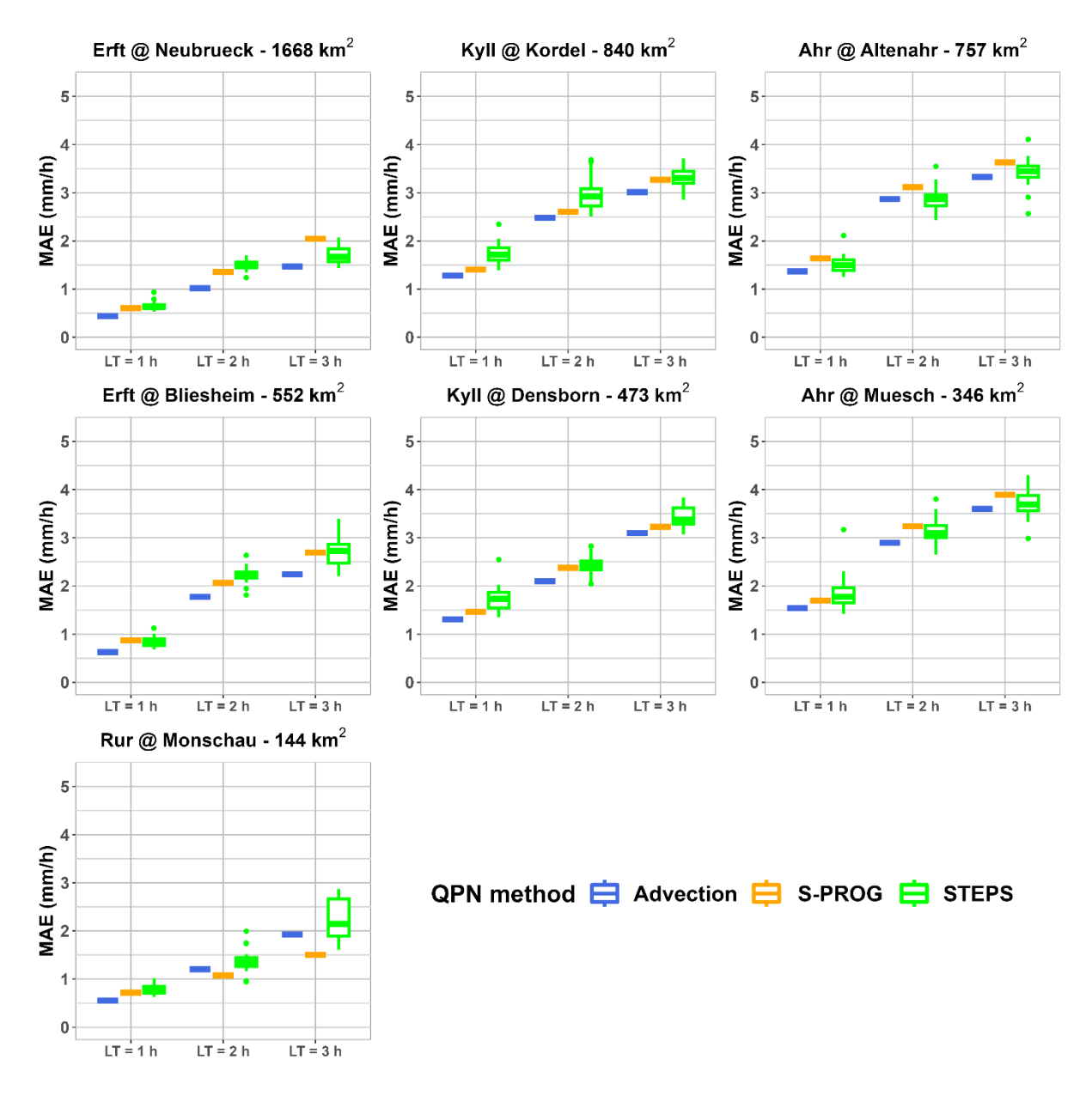


Fig. 5. Mean absolute errors between observed precipitation (QPE) and QPN estimated using advection, S-PROG, and STEPS at the scale of each catchment. LT refers to lead time.

b. Added hydrological value of QPN

To investigate the added value of the tested QPN methods from a hydrological point of view, we first show in subsection 4.b.1 the hindcasted hydrographs using RADOLAN and the QPE product RAVKDP for the 14 July 2021 event (Fig. 6) based on which the quality of the forecasted hydrographs is estimated using NSE (Fig. 7). Second, in subsection 4.b.2, we show the skill of the QPN methods computed using the CRPS between the corresponding forecasted hydrographs and the hindcasted hydrograph using QPE, with respect to the benchmarks of the hydrological persistence or the zero-precipitation nowcasts (Figs. 8 and 9).

137	Finally, in subsection 4.b.3, we show the gains in lead time obtained using either the
438	efficiency-based approach (with NSE) or the skill-based approach (with CRPS) and
139	depending on the benchmark (hydrological persistence or zero-precipitation nowcasts; Fig.
440	10).
441	1) HINDCASTED HYDROGRAPHS AND QUALITY OF THE FORECASTED HYDROGRAPHS
142	To illustrate the dynamics of the catchment responses to the extreme rainfall event of 14
143	July 2021, simulated hydrographs using RADOLAN (prior to 14 July 2021) and the QPE
144	product RAVKDP (for 14 July 2021) by GR4H and ParFlowCLM are presented in Fig. 6.
145	They indicate that the highest recorded peak flow prior to July 2021 (in orange dashed lines)
146	was surpassed by model simulations at least once in all the catchments except the Rur at
147	Monschau. However, where available, the last measured peak flow before the unavailability
148	of records was surpassed by model simulations only for the catchments drained by the Ahr
149	river. Qualitatively, GR4H and ParFlowCLM agreed for the catchments drained by the Ahr
450	and the Kyll, whereas they significantly disagreed over the Erft and the Rur. Finally, the
451	spread in the GR4H simulations reflects the large uncertainty in simulated hydrographs due
452	to parameter uncertainty (Saadi et al. 2023).

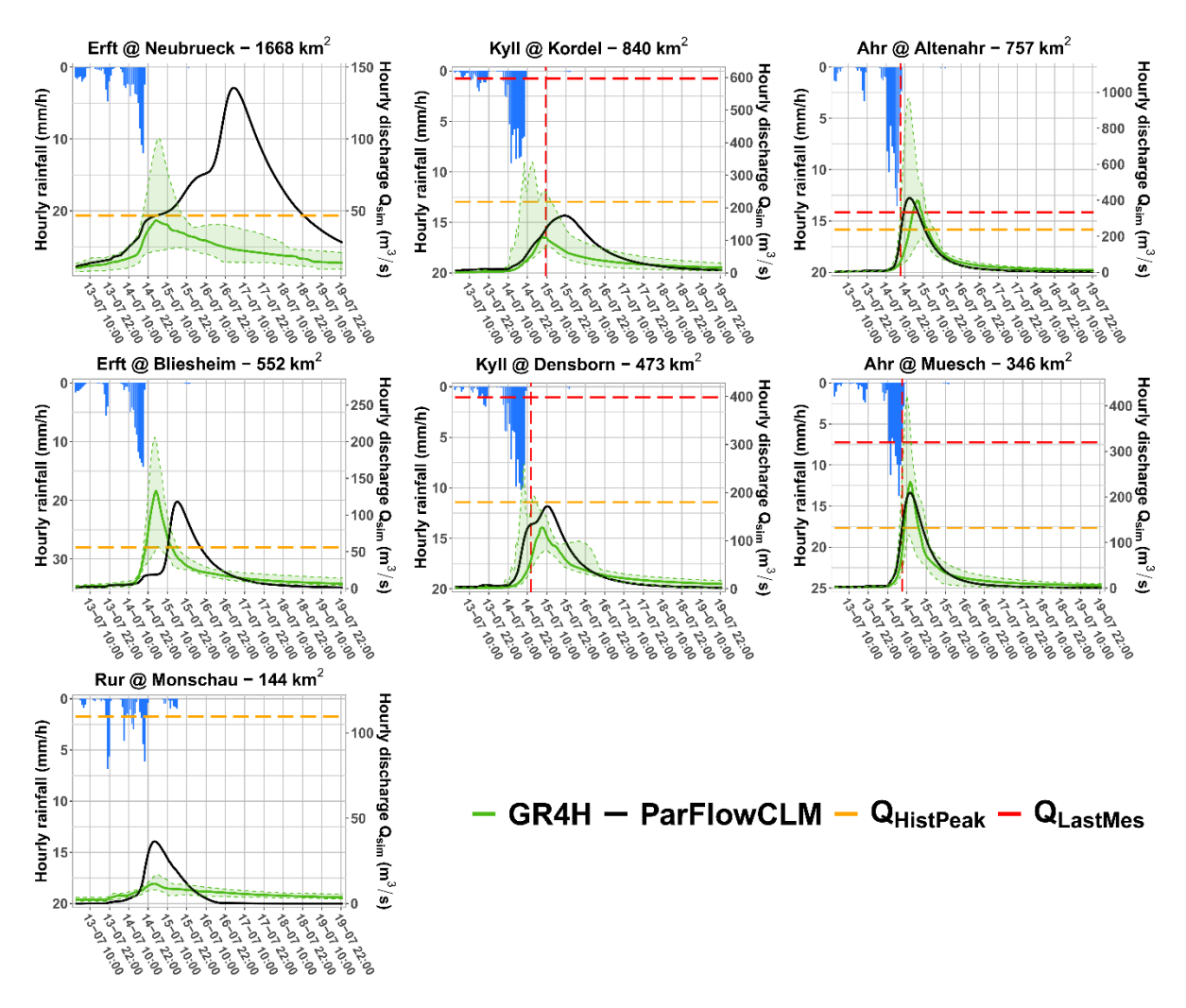


Fig. 6. Simulated hydrographs for the July 2021 events using 12 parameter sets with GR4H (shaded area in green) and one parameter set with ParFlowCLM (in black). Orange dashed lines indicate the highest recorded peak flow (Q_{HistPeak}) prior to July 2021. Subject to availability, red dashed horizontal lines indicate the reported last measured peak flows before the failure of the monitoring devices (Q_{LastMes}), and red dashed vertical lines their timings. Hydrographs are simulated using the QPE product RAVKDP on 14 July 2021 and RADOLAN for the remaining time steps. For GR4H, the shaded area is delimited by the minmax of the simulations at each time step using 12 parameter sets for each catchment.

From the hydrological viewpoint, the three QPN methods yielded very similar hydrological forecasts across the seven catchments, as suggested by their NSE scores in Fig. 7. At the threshold of NSE_{th} = 0.9, the three methods yielded satisfactory hydrological forecasts for lead times ranging from 1 up to 5 h (GR4H for the Erft at Neubrueck, ParFlowCLM for the Rur at Monschau). The benchmark of the hydrological persistence (Q) obtained the fastest decreasing NSE curves, which is expected given its limits for a highly variable catchment response during the event. However, the benchmark of the zero-precipitation nowcasts (ZNC) succeeded in yielding better hydrological forecasts using ParFlowCLM for the catchments drained by the Kyll. For these two catchments, the use of

the QPN products led to early increases of the forecasted hydrographs with respect to the hindcasted hydrograph, resulting in deteriorated NSE values compared with the ZNC benchmark in the early lead times. Finally, the QPN methods led to more satisfactory hydrological forecasts when using GR4H than when using ParFlowCLM, except for the Rur at Monschau.

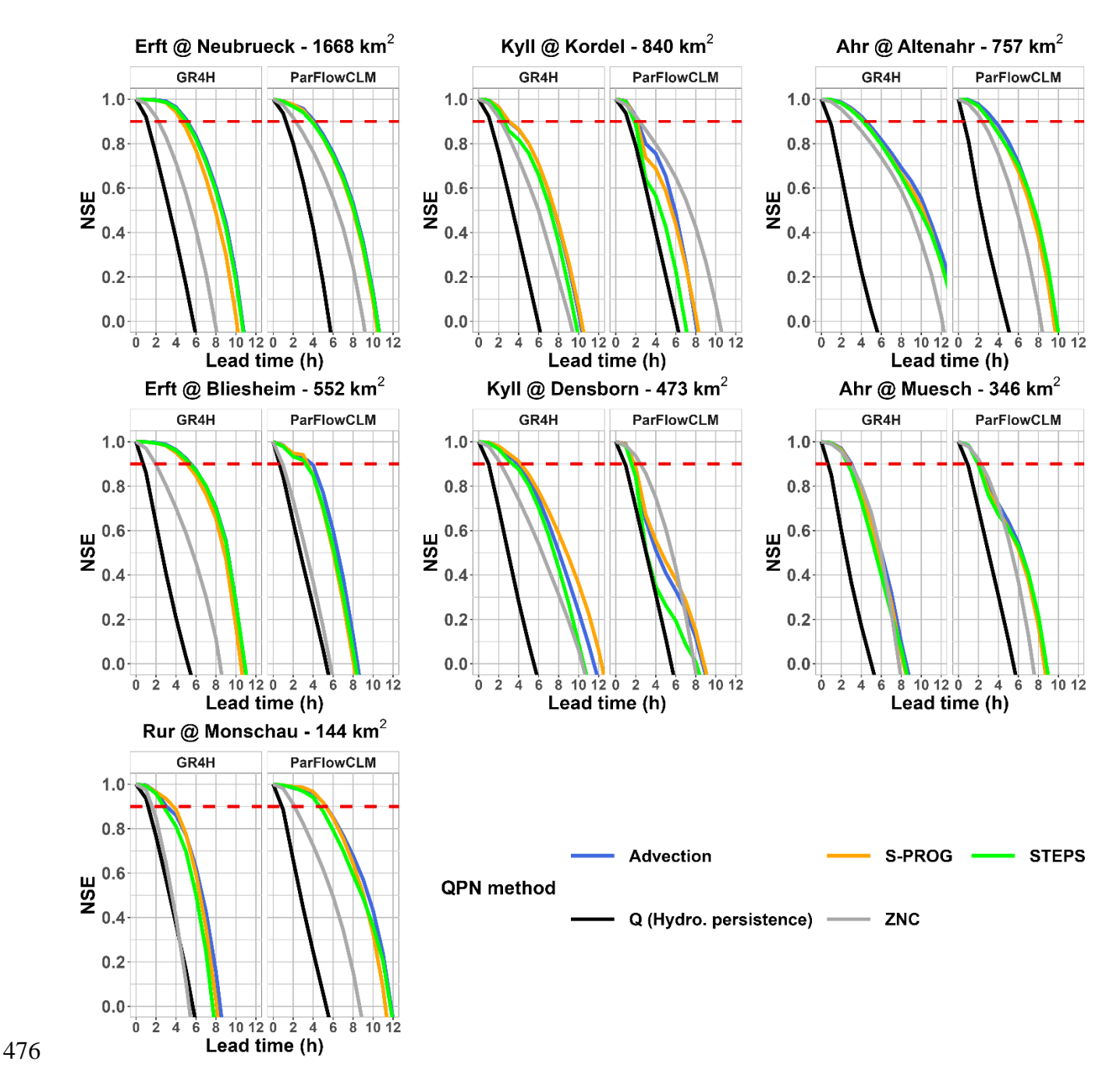


Fig. 7. Evolution of the Nash-Sutcliffe Efficiency (NSE) of the forecasted hydrographs using the QPN methods and the benchmarks (hydrological persistence Q, zero-precipitation nowcasts ZNC) with respect to lead time. Red dashed lines indicate the NSE threshold NSE $_{th}$ = 0.9. For GR4H, the curves represent the median score from the 12 simulations. For STEPS, the curves represent the median score from the 20 members.

2) SKILL OF THE QPN METHODS

The three QPN methods were also similar in terms of their skill with respect to the benchmark of hydrological persistence, as can be seen in Fig. 8. The skill indicates that using QPN yielded better forecasts than the persistence model for lead times higher than 30 h, except for the Rur at Monschau where the skill dropped after only 16 h. Note that this should be interpreted in the light of the quality of the forecasted hydrographs by both the QPN methods and the benchmark of the hydrological persistence, which in all cases had negative NSE values after a lead time of 12 h (see Fig. 7). The evolution of the skill was somewhat distinct for each catchment, but similar for the catchments drained by the same river, which indicates a dependency on location with respect to the precipitation event. The rebound in the skill curve for the catchments drained by the Ahr river may reflect the change in the forecasted part of the hydrograph from the rising to the falling limb. Finally, both models showed similar evaluation of the three QPN methods, with GR4H showing slightly higher skill scores than ParFlowCLM at the very short lead times.

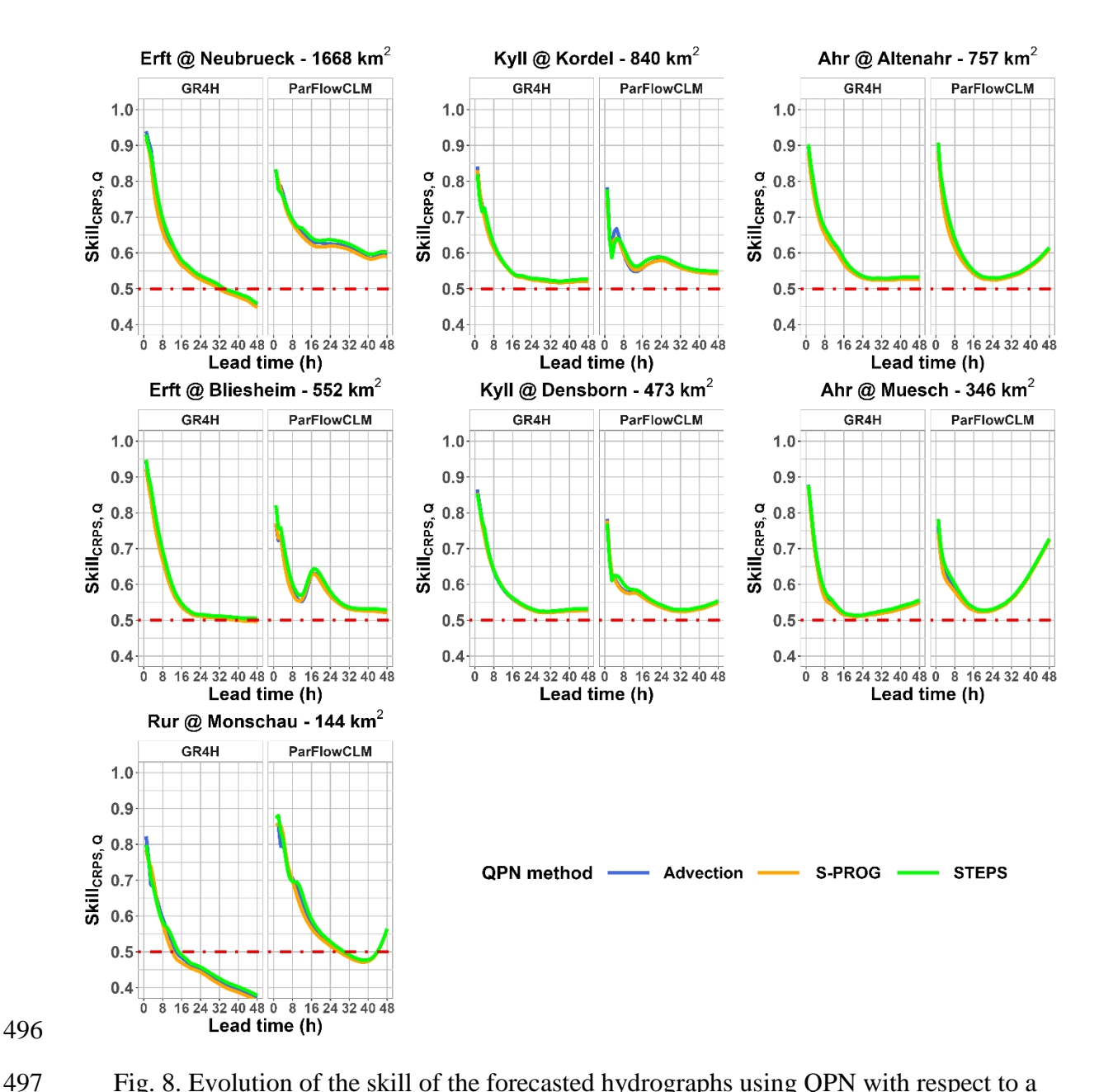


Fig. 8. Evolution of the skill of the forecasted hydrographs using QPN with respect to a hydrological persistence benchmark (Skill_{CPRS, Q}) over the seven catchments. Dashed red lines indicate a skill of 0.5, i.e. using QPN is as good as the hydrological persistence model. For GR4H, the curves represent the median score from the 12 simulations.

Changing the benchmark to zero-precipitation nowcasts (ZNC) had a limited impact on the skill of the tested QPN, as suggested by Fig. 9. Namely, the skill slightly decreased compared with the hydrological persistence in Fig. 8, indicating that the ZNC is a more challenging benchmark to beat than the hydrological persistence. This is somewhat expected given the better performances of ZNC compared with hydrological persistence, as can be seen in Fig. 7. This is not however the case for all catchments. The Rur at Monschau indicates that the ZNC benchmark is easier to outperform than the hydrological persistence.

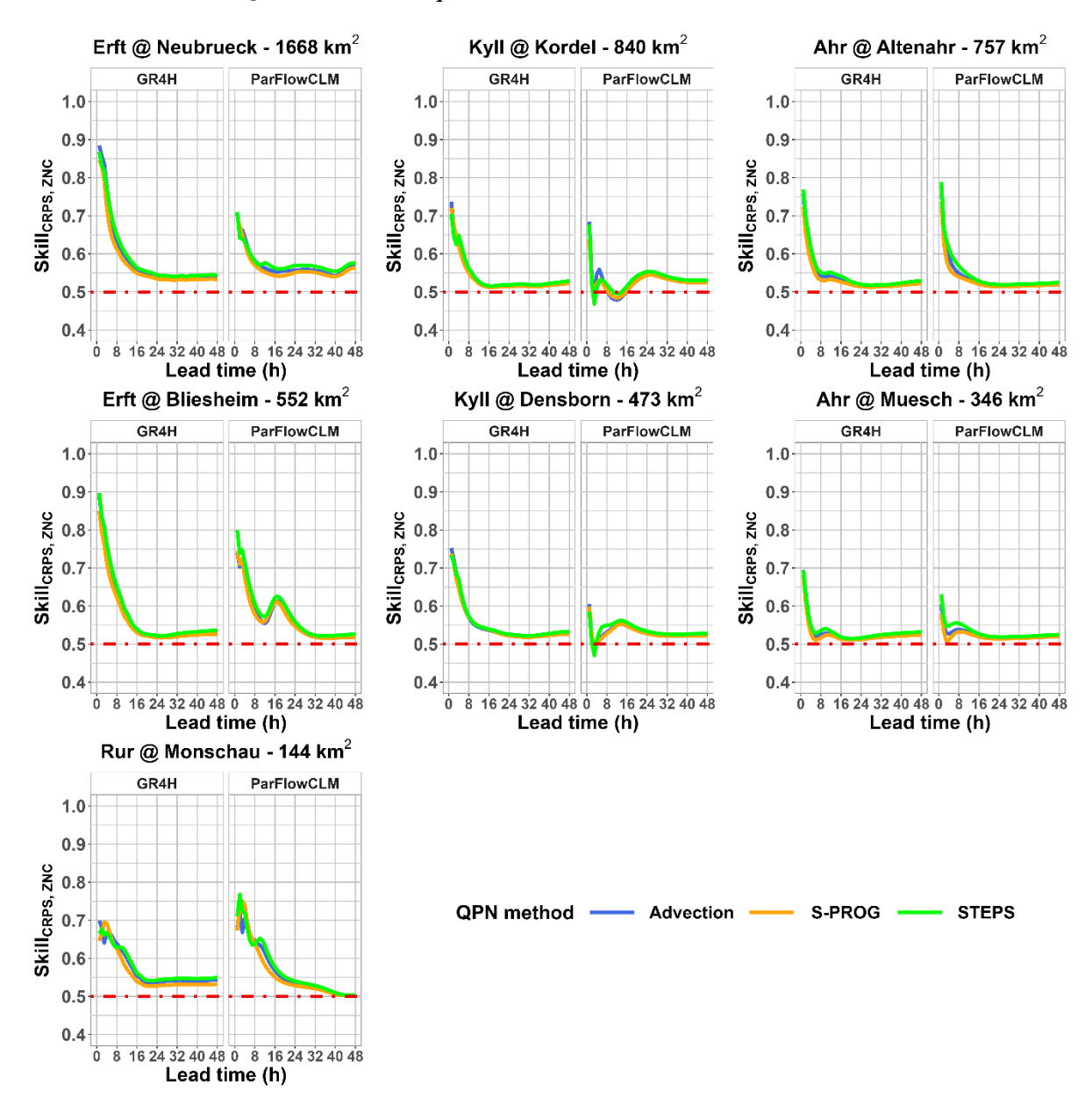


Fig. 9. Evolution of the skill of the forecasted hydrographs using QPN with respect to forecasted hydrographs with zero-precipitation nowcasts (ZNC). Red dashed lines indicate a skill of 0.5, i.e. using QPN is as good as feeding the models with ZNC. For GR4H, the curves represent the median score from the 12 simulations.

3) GAINS IN LEAD TIME WITH RESPECT TO THE BENCHMARKS

The gain in lead time reflects the dependency on the evaluation method, the benchmark and the chosen threshold for NSE or for the skill, as shown in Fig. 10. Based on NSE and for a threshold at $NSE_{th} = 0.9$ (Figs. 10a and 10b), gains in lead time ranged between 1 h and 5 h with GR4H (on average) and between 0 h and 5 h with ParFlowCLM with respect to the

hydrological persistence. With respect to ZNC, gains ranged between 0 h and 4 h with GR4H (on average) and in some cases there were losses with ParFlowCLM, specifically in the catchments drained by the Kyll and the Ahr at Muesch. Changing the threshold from NSE_{th} = 0.9 to NSE_{th} = 0.5 led to increases in the gains only with respect to the hydrological persistence (Figs. 10c and 10d). In this case, the gains ranged between 2 h and 8 h with GR4H and between 0 h and 7 h with ParFlowCLM. With respect to ZNC, changing the NSE threshold from 0.9 to 0.5 resulted in poorer gains, especially for ParFlowCLM (range: -3 h to 4 h). This is caused by faster decreases in the quality of the forecasted hydrographs with the QPN methods compared with those forecasted with ZNC (Fig. 7)

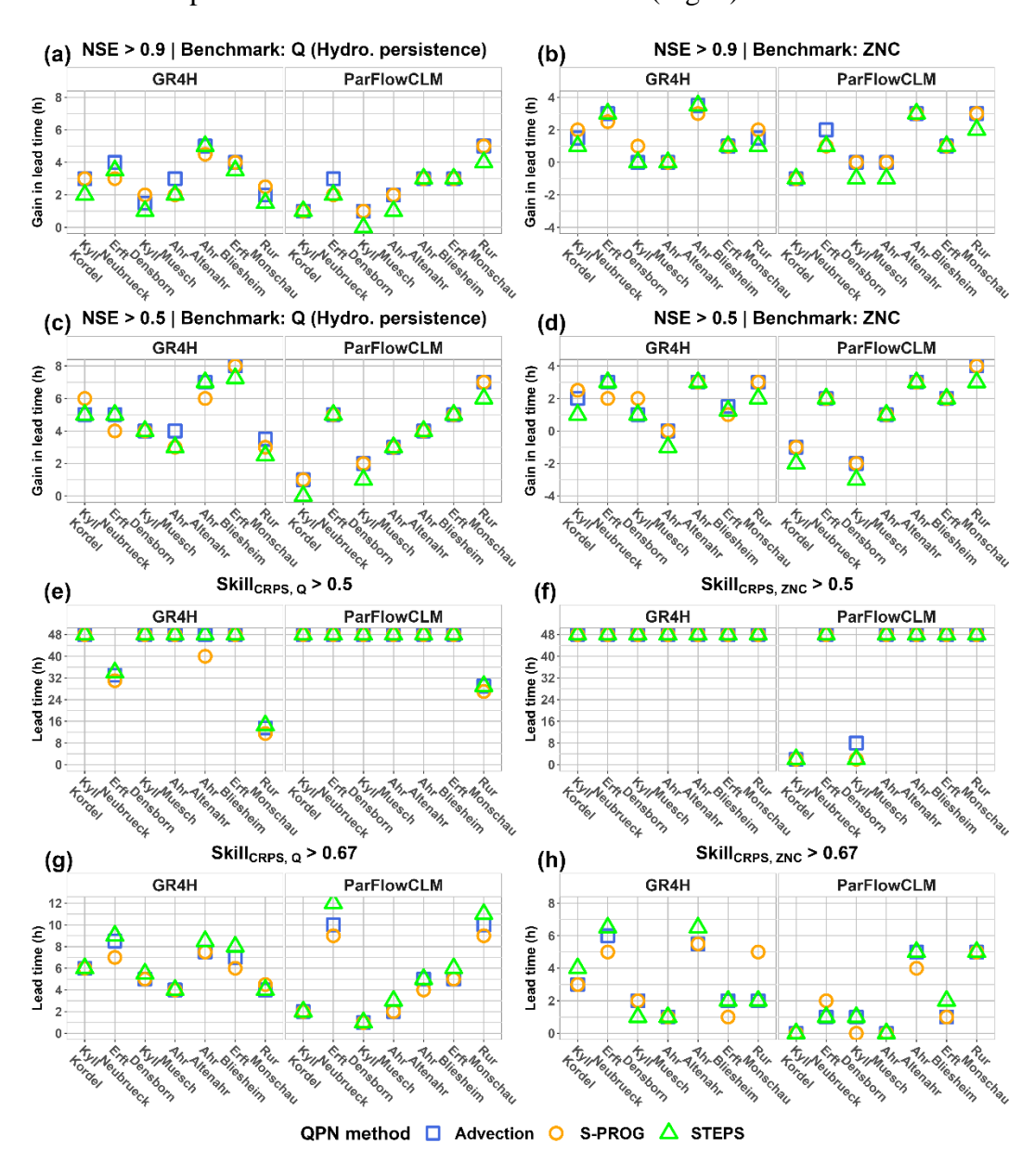


Fig. 10. Gain in lead time based on Nash-Sutcliffe score with respect to hydrological persistence (on the left) and zero-precipitation nowcasts (on the right) as benchmarks with a

score threshold at 0.9 for (a) and (b), and at 0.5 for (c) and (d). Lead time (in hours) up to which using QPN was better than the benchmark (hydrological persistence on the left, zeroprecipitation nowcasts on the right) according to a skill threshold at 0.5 for (e) and (f), and at 0.67 for (g) and (h). On the x-axis, catchments are ranked with decreasing Gravelius index from left to right. Note that the evolution of the skills was computed up to a maximum of 48 Using the skill-based approach, choosing the default threshold (0.5, Figs. 10e and 10f) yielded much larger gains in lead time compared with a more demanding threshold (0.67,

Figs. 10g and 10h). With a threshold of 0.5 (Figs. 10e and 10f), the improvements were up to 48 h, the maximum range to which we limited our analysis, which should be interpreted in the light of the poor performances of the benchmarks (Fig. 7). With a threshold of 0.67, the use of QPN improved the forecast lead time by 4 h up to 9 h with GR4H, and by 1 h up to 12

h with ParFlowCLM (Erft at Neubrueck, the largest catchment) with respect to the hydrological persistence as benchmark (Fig. 10g). With respect to ZNC (Fig. 10h), the

improvements ranged between 1 h and 7 h with GR4H and between 0 h and 5 h with

547 ParFlowCLM.

Finally, we found no consistent pattern in the gains in lead time with respect to catchment area (not show here). However, when the catchments are ranked by their Gravelius index (Eq. 8), the added value of the QPN methods with respect to the hydrological persistence using ParFlowCLM increased as the Gravelius index decreased (Figs. 10a, 10c and 10g). This suggests that with ParFlowCLM, using the QPN methods was more beneficial for catchments with a more compact shape. This dependency on the catchment shape was not detectable with GR4H.

5. Discussion

For the major flooding event of July 2021 in our study region, the three tested QPN products obtained very similar performances in terms of both the reproduction of observed precipitation and hydrological forecasting. The highly similar performances of the three methods can be attributed to two factors. First, the aggregation to the hourly time step may have filtered out the differences between the three methods, which are reported by previous studies to be in the order of few to tens of minutes (Ayzel et al. 2019; Berenguer et al. 2005; Heuvelink et al. 2020; Imhoff et al. 2020). Fig. 3 shows however that the methods are already similar at 5-min resolution, with a slightly better performance for S-PROG. Second, the persistent nature of the event (see event hyetographs in Fig. 6) might have made it as easy to

565	be forecasted by simple nowcasting methods (advection) as by more sophisticated ones (S-
566	PROG and STEPS). The poor performances of the STEPS ensemble compared with the
567	ensemble mean STEPS-m suggests that the perturbations of the deterministic forecast got
568	penalized for this event (Heuvelink et al. 2020). In addition, comparing the spread in the
569	STEPS ensemble with the deterministic STEPS-m or S-PROG forecasts suggests that the
570	STEPS ensemble might have underestimated the uncertainty in the evolution of the
571	precipitation field for this event (Foresti et al. 2016). Nevertheless, the similarity in terms of
572	performances between STEPS and the deterministic methods should not undermine its
573	benefits in providing probabilistic nowcasts, which are of greater value for decision makers
574	than deterministic ones (Fundel et al. 2019; Merz et al. 2020).
575	Overall, our results show that the QPN methods improved the hydrological forecasts
576	compared with hydrological persistence or with the zero-precipitation nowcasts. Previous
577	studies such as Heuvelink et al. (2020), Berenguer et al. (2005), and Vivoni et al. (2006)
578	reported improvements of 2 to 6 h for catchments of $\sim 10^3 \text{ km}^2$ of size. First, some of the
579	differences may be explained by the hydroclimatic settings of the studied catchments and/or
580	their characteristic response times (or concentration times). Berenguer et al. (2005) studied
581	catchments located in the Mediterranean region (north-east of Spain), for which the fast
582	response may explain the absence of significant improvements using QPN beyond 2 h. On
583	the contrary, Heuvelink et al. (2020) showed that significant improvements in the
584	hydrological forecasts can be obtained when using 3-h long QPN for catchments under
585	humid, temperate climate (Netherlands) and characterized by slower responses than
586	Mediterranean catchments. In our case, the improvements are in general limited to 4 h with
587	respect to a benchmark of zero-precipitation nowcasts, with a high variability from one
588	catchment to another (Figs. 10b and 10d). For some catchments (drained by the Kyll and the
589	Ahr at Muesch), the QPN methods showed worse performances compared with the zero-
590	precipitation nowcasts, especially with ParFlowCLM. The variability in the performances of
591	the QPN from one catchment to another can be either explained by the location of each
592	catchment within the precipitation field, or their properties that modulate the delay between
593	the precipitation and the catchment response.
594	Second, some of the differences can be attributed to methodological choices. Using the
595	same approach as in Heuvelink et al. (2020) and Berenguer et al. (2005) based on the quality
596	of the forecasted hydrographs measured by NSE, we obtained similar improvements up to 4-5

598	this NSE-based approach suffers from the arbitrary selection of an efficiency threshold,
599	which, according to Figs. 10a to 10d, impacted the estimation of the added value of QPN,
600	especially with respect to the hydrological persistence as benchmark. We attempted to
601	circumvent this issue by following a skill-based approach, which provides an a-priori
602	objective threshold (i.e., 0.5, see Eq. 7), but leads to too optimistic results and suggests that
603	the skill of QPN lasts for much longer lead times (Figs. 8 and 9, except for the Rur at
604	Monschau in Fig. 8 and the catchments drained by the Kyll in Fig. 9). By adopting a more
605	demanding threshold such as 0.67, our skill-based approach leads to results that agree with
606	previous studies (Figs. 10g and 10h; Heuvelink et al. 2020; Berenguer et al. 2005). The
607	combination of a skill-based approach with an analysis of the quality of forecasted
608	hydrographs helped objectively estimate the added value of the QPN products and avoid a
609	distorted evaluation when the benchmark performs poorly. In all cases, the obtained
610	improvements may look small, but they can still be of high value for emergency management
611	and the fire services involved in event response (Speight et al. 2021). However, if observed
612	hydrographs of the event were available and used, they would probably have led to lower
613	added value of QPN because of additional errors resulting from the disagreement between the
614	QPE product and corresponding hindcasted hydrographs with the observed precipitation and
615	observed hydrographs, respectively.
616	Several studies reported a dependency of improvements on the catchment size and the
617	event type (convective vs. stratiform; Berenguer et al., 2005; Heuvelink et al., 2020; Imhoff
618	et al., 2020). We showed that, in addition, there is also a dependency on methodological
619	choices, namely the chosen benchmark and the applied hydrological model. The dependency
620	on the benchmark used to estimate the skill was visible (albeit to a limited extent) from
621	comparing Figs. 8 and 9, which warns that choosing a simple model (such as hydrological
622	persistence) may lead to overly optimistic interpretations of the improvements (Pappenberger
623	et al. 2015b). The dependency on catchment size was hardly visible over our catchment set
624	for the studied event, except for the largest catchment (Erft at Neubrueck, 1668 km²) which
625	showed a slow decrease in the skill with respect to lead time. The low sensitivity of the skills
626	to catchment size is perhaps a result of working on a single event, which emphasizes the
627	impact of the differences of precipitation amounts registered in the study catchments.
628	Nevertheless, we noticed a dependency on catchment shape when the hydrological

persistence is chosen as benchmark and with ParFlowCLM as a hydrological model (Figs.

h with an NSE threshold at 0.9, depending on the benchmark (Figs. 10a and 10b). However,

597

630	10a, 10c and 10g), but not with GR4H. The fact that GR4H did not mirror the effect of
631	catchment shape can be explained by the sensitivity of GR4H parameters to the
632	anthropogenic effects through calibration on historical observations (Saadi et al. 2020), which
633	are behind the large differences between model simulations for the Erft at Neubrueck and the
634	Rur at Monschau in Fig. 6. Accounting for the anthropogenic effects by GR4H (even
635	implicitly) may have buffered the effect of catchment shape on the catchment response.
636	The dependency of the skill on the catchment response, i.e. the event hydrograph, was
637	accentuated by the adoption of the hydrological persistence as benchmark. Since the
638	reference event hydrograph is the one simulated by the hydrological models using the QPE,
639	the NSE curves in Fig. 7 suggest that the flashier and the higher the hindcasted peak flow, the
640	higher the benefit of the use of QPN. This can be seen from comparing the hindcasted
641	hydrographs by GR4H and ParFlowCLM for the Erft at Bliesheim (Fig. 6), where GR4H
642	hindcasted an earlier peak flow than ParFlowCLM, mirrored by better NSE values for the
643	three QPN methods when GR4H was applied for this catchment (Fig. 7). Conversely, the
644	simulated hydrograph by GR4H for the Rur at Monschau was smoother than the one
645	simulated by ParFlowCLM, which was accompanied by better gains in lead times for QPN
646	with ParFlowCLM (Fig. 7). The smoother hydrographs led to less gains because the use of
647	QPN led to earlier rises in the forecasted hydrographs, which penalized their use. These
648	differences also reflect the errors of QPN with respect to the QPE product, which are
649	highlighted by the distributed ParFlowCLM for the catchments drained by the Kyll, where
650	the zero-precipitation nowcasts showed similar or better NSE scores at the early time steps
651	(Fig. 7).
652	Nevertheless, the choice of the adopted hydrological model did not much alter the
653	conclusions regarding the similarity of the tested QPN methods. The agreement between
654	QPN according to the distributed ParFlowCLM model suggests that the methods agreed also
655	in the spatial distribution of precipitation for this particular event at least from a hydrological
656	point of view, in line with the MAE patterns in Fig. 4. Effects of uncertainties in parameter
657	estimation of the hydrological models were not included here, but they would be relatively
658	low given the general agreement of the three methods in terms of predicting the observed
659	QPE. Effects of uncertainties in initial moisture conditions were minimized by the long spin-
660	up period of both GR4H and ParFlowCLM models prior to the event.

Focusing only on one event limits our investigation of other factors that could have impacted the skill of the tested nowcasting methods, such as the type of the event and the season (Imhoff et al. 2020). The absence of observed discharge values limits the evaluation of the accuracy of model simulations, but that should not undermine the obtained improvements by the use of QPN. Quantifying the added value of the tested QPN with respect to a NWP-based benchmark for this event would give more convincing results from an operational point of view, given the relative poorness of the adopted benchmarks in our study. Finally, the relatively heavy cost of model simulations with ParFlowCLM (especially when applied with the probabilistic STEPS nowcasts) hampers its test with more parameter sets, which could have an impact on the evaluation of the skill, especially with respect to the hydrological persistence as a benchmark.

6. Conclusions and future work

We investigated the usefulness of using precipitation nowcasts to improve the skill of two hydrological models in forecasting the response of seven catchments located in the west of Germany for the disastrous July 2021 event. We evaluated three precipitation nowcasting techniques, namely the Lagrangian advection, S-PROG, and the probabilistic method STEPS. Our evaluation consisted of analyzing their ability in forecasting the observed precipitation at 5-min and hourly time steps, then in improving the ability of two contrasting hydrological models, GR4H and ParFlowCLM, in reproducing the simulated hydrographs by the hydrological models using observed precipitation (or hindcasted hydrographs). For the July 2021 events in our study region, our main conclusions are:

- 1. The three methods improved the forecasting skill of the hydrological models with respect to two benchmarks, the hydrological persistence and the zero-precipitation nowcasts. These improvements varied from one catchment to another, and reached up to 4-5 h according to an NSE at 0.9 and up to 12 h according to the CRPS skill at a threshold of 0.67 (i.e., the use of QPN halved the forecasting errors of the benchmarks).
- The three methods obtained very similar performances in terms of both
 precipitation and discharge forecasting. In particular, the deterministic methods
 (advection and S-PROG) performed as good as the average/median probabilistic
 one (STEPS).

- 3. The use of a conceptual, lumped model (GR4H) led to similar conclusions as with a physically-based, 3D-distributed model (ParFlowCLM). However, the gains in lead time were on average lower with ParFlowCLM than with GR4H. The differences between the two models can be attributed to the anthropogenic influences in the catchments, which are implicitly accounted for by GR4H through its calibrated parameters on historical observations.
 - 4. The choice of the evaluation method, the benchmark and the skill threshold impacted the estimation of the added value of the QPN methods.

As future work, more robust conclusions would be obtained by considering a large sample of events with a variety of seasons and typologies. Increasing the horizon of the input precipitation to the models with quantitative precipitation forecasts that make use of (convection-permitting) NWP outputs through blending approaches (Lovat et al. 2022; Speight et al. 2021; Clark et al. 2016) would shed more light on the ability of the current hydrometeorological chains in hedging the damages by issuing useful and timely flood warnings. Quantifying the economic gains from including precipitation nowcasts (Le Bihan et al. 2017; Pappenberger et al. 2015a) would provide more convincing arguments about their usefulness. Finally, the added value of the nowcasting techniques presented in this work motivates to exploit their benefit in generating nationwide and useful short-time forecasts for better disaster preparedness (Reinoso-Rondinel et al. 2022).

711 Acknowledgments.

This study is part of the RealPEP (Near-Realtime Quantitative Precipitation Estimation and Prediction https://www2.meteo.uni-bonn.de/realpep/doku.php) P4 project (Evaluation of QPE and QPN improvements in a flash flood nowcasting framework with data assimilation), funded by the *Deutsche Forschungsgemeinschaft* (German Research Foundation). The authors gratefully acknowledge the Earth System Modeling Project (ESM) for funding this work by providing computing time for ParFlowCLM runs on the ESM partition of the supercomputer JUWELS at the Jülich Supercomputing Centre (JSC). The authors declare they have no conflict of interest.

Data Availability Statement.

All original data are public, except for the QPN and the QPE products generated for the study, which can be made available upon reasonable request from the authors.

723	REFERENCES
724 725 726	Abrams, M., R. Crippen, and H. Fujisada, 2020: ASTER Global Digital Elevation Model (GDEM) and ASTER Global Water Body Dataset (ASTWBD). <i>Remote Sensing</i> , 12 , 1156, https://doi.org/10.3390/rs12071156.
727 728 729	Alfieri, L., P. Salamon, F. Pappenberger, F. Wetterhall, and J. Thielen, 2012: Operational early warning systems for water-related hazards in Europe. <i>Environmental Science & Policy</i> , 21 , 35–49, https://doi.org/10.1016/j.envsci.2012.01.008.
730 731 732	Atencia, A., and I. Zawadzki, 2014: A Comparison of Two Techniques for Generating Nowcasting Ensembles. Part I: Lagrangian Ensemble Technique. <i>Monthly Weather Review</i> , 142 , 4036–4052, https://doi.org/10.1175/MWR-D-13-00117.1.
733 734 735	——, and ——, 2015: A Comparison of Two Techniques for Generating Nowcasting Ensembles. Part II: Analogs Selection and Comparison of Techniques. <i>Monthly Weather Review</i> , 143 , 2890–2908, https://doi.org/10.1175/MWR-D-14-00342.1.
736 737 738 739	Auger, L., O. Dupont, S. Hagelin, P. Brousseau, and P. Brovelli, 2015: AROME–NWC: a new nowcasting tool based on an operational mesoscale forecasting system. <i>Quarterly Journal of the Royal Meteorological Society</i> , 141 , 1603–1611, https://doi.org/10.1002/qj.2463.
740 741 742	Ayzel, G., M. Heistermann, and T. Winterrath, 2019: Optical flow models as an open benchmark for radar-based precipitation nowcasting (rainymotion v0.1). <i>Geoscientific Model Development</i> , 12 , 1387–1402, https://doi.org/10.5194/gmd-12-1387-2019.
743 744	Bauer, P., A. Thorpe, and G. Brunet, 2015: The quiet revolution of numerical weather prediction. <i>Nature</i> , 525 , 47–55, https://doi.org/10.1038/nature14956.
745 746 747 748	Belleflamme, A., and Coauthors, 2023: Hydrological forecasting at impact scale: the integrated ParFlow hydrological model at 0.6 km for climate resilient water resource management over Germany. <i>Frontiers in Water</i> , 5 , https://doi.org/10.3389/frwa.2023.1183642.
749 750 751	Bendjoudi, H., and P. Hubert, 2002: The Gravelius compactness coefficient: critical analysis of a shape index for drainage basins. <i>Hydrological Sciences Journal</i> , 47 , 921–930, https://doi.org/10.1080/02626660209493000.
752 753 754	Berenguer, M., C. Corral, R. Sánchez-Diezma, and D. Sempere-Torres, 2005: Hydrological Validation of a Radar-Based Nowcasting Technique. <i>Journal of Hydrometeorology</i> , 6 532–549, https://doi.org/10.1175/JHM433.1.
755 756 757	—, D. Sempere-Torres, and G. G. S. Pegram, 2011: SBMcast – An ensemble nowcasting technique to assess the uncertainty in rainfall forecasts by Lagrangian extrapolation. <i>Journal of Hydrology</i> , 404 , 226–240, https://doi.org/10.1016/j.jhydrol.2011.04.033.
758 759 760	——, M. Surcel, I. Zawadzki, M. Xue, and F. Kong, 2012: The Diurnal Cycle of Precipitation from Continental Radar Mosaics and Numerical Weather Prediction Models. Part II: Intercomparison among Numerical Models and with Nowcasting.

761	Monthly Weather Review, 140, 2689–2705, https://doi.org/10.1175/MWR-D-11-
762	00181.1.

- 763 Berthet, L., V. Andréassian, C. Perrin, and P. Javelle, 2009: How crucial is it to account for 764 the antecedent moisture conditions in flood forecasting? Comparison of event-based 765 and continuous approaches on 178 catchments. Hydrology and Earth System Sciences, 13, 819–831, https://doi.org/10.5194/hess-13-819-2009. 766
- Bowler, N. E., C. E. Pierce, and A. W. Seed, 2006: STEPS: A probabilistic precipitation 767
- forecasting scheme which merges an extrapolation nowcast with downscaled NWP. 769 Quarterly Journal of the Royal Meteorological Society, 132, 2127–2155,
- 770 https://doi.org/10.1256/qj.04.100.

- 771 Chen, C., J. Twycross, and J. M. Garibaldi, 2017: A new accuracy measure based on bounded 772 relative error for time series forecasting. *PLOS ONE*, **12**, e0174202, 773 https://doi.org/10.1371/journal.pone.0174202.
- Chen, J.-Y., S. Trömel, A. Ryzhkov, and C. Simmer, 2021: Assessing the Benefits of Specific 774 Attenuation for Quantitative Precipitation Estimation with a C-Band Radar Network. 775 776 Journal of Hydrometeorology, 22, 2617–2631, https://doi.org/10.1175/JHM-D-20-777 0299.1.
- 778 —, R. Reinoso-Rondinel, S. Trömel, C. Simmer, and A. Ryzhkov, 2022: A Radar-Based 779 Quantitative Precipitation Estimation Algorithm to Overcome the Impact of Vertical 780 Gradients of Warm-Rain Precipitation: the Flood in Western Germany on 14 July 2021. Journal of Hydrometeorology, 1, https://doi.org/10.1175/JHM-D-22-0111.1. 781
- 782 Clark, P., N. Roberts, H. Lean, S. P. Ballard, and C. Charlton-Perez, 2016: Convection-783 permitting models: a step-change in rainfall forecasting. *Meteorological Applications*, 784 23, 165–181, https://doi.org/10.1002/met.1538.
- 785 Cloke, H. L., and F. Pappenberger, 2009: Ensemble flood forecasting: A review. *Journal of Hydrology*, **375**, 613–626, https://doi.org/10.1016/j.jhydrol.2009.06.005. 786
- 787 Coron, L., G. Thirel, O. Delaigue, C. Perrin, and V. Andréassian, 2017: The suite of lumped 788 GR hydrological models in an R package. Environmental Modelling and Software, 94, 166–171, https://doi.org/10.1016/j.envsoft.2017.05.002. 789
- 790 Dottori, F., and Coauthors, 2018: Increased human and economic losses from river flooding 791 with anthropogenic warming. Nature Clim Change, 8, 781–786, 792 https://doi.org/10.1038/s41558-018-0257-z.
- 793 Dougherty, E., and K. L. Rasmussen, 2020: Changes in Future Flash Flood-Producing 794 Storms in the United States. *Journal of Hydrometeorology*, **21**, 2221–2236, 795 https://doi.org/10.1175/JHM-D-20-0014.1.
- 796 Duscher, K., A. Günther, A. Richts, P. Clos, U. Philipp, and W. Struckmeier, 2015: The GIS 797 layers of the "International Hydrogeological Map of Europe 1:1,500,000" in a vector 798 format. Hydrogeol J, 23, 1867–1875, https://doi.org/10.1007/s10040-015-1296-4.

799	Edijatno, N. de O. Nascimento, X. Yang, Z. Makhlouf, and C. Michel, 1999: GR3J: a daily
800	watershed model with three free parameters. Hydrological Sciences Journal, 44, 263-
801	277, https://doi.org/10.1080/02626669909492221.

- Ficchì, A., C. Perrin, and V. Andréassian, 2019: Hydrological modelling at multiple sub-daily time steps: Model improvement via flux-matching. *Journal of Hydrology*, **575**, 1308–1327, https://doi.org/10.1016/j.jhydrol.2019.05.084.
- Foresti, L., L. Panziera, P. V. Mandapaka, U. Germann, and A. Seed, 2015: Retrieval of analogue radar images for ensemble nowcasting of orographic rainfall.

 Meteorological Applications, 22, 141–155, https://doi.org/10.1002/met.1416.
- Foresti, L., M. Reyniers, A. Seed, and L. Delobbe, 2016: Development and verification of a real-time stochastic precipitation nowcasting system for urban hydrology in Belgium.

 Hydrology and Earth System Sciences, 20, 505–527, https://doi.org/10.5194/hess-20-505-2016.
- Fowler, H. J., and Coauthors, 2021: Anthropogenic intensification of short-duration rainfall extremes. *Nat Rev Earth Environ*, **2**, 107–122, https://doi.org/10.1038/s43017-020-00128-6.
- Fundel, V. J., N. Fleischhut, S. M. Herzog, M. Göber, and R. Hagedorn, 2019: Promoting the use of probabilistic weather forecasts through a dialogue between scientists, developers and end-users. *Quarterly Journal of the Royal Meteorological Society*, 145, 210–231, https://doi.org/10.1002/qj.3482.
- Germann, U., and I. Zawadzki, 2002: Scale-Dependence of the Predictability of Precipitation from Continental Radar Images. Part I: Description of the Methodology. *Mon. Wea. Rev.*, **130**, 2859–2873, https://doi.org/10.1175/1520-0493(2002)130<2859:SDOTPO>2.0.CO;2.
- Hengl, T., and Coauthors, 2017: SoilGrids250m: Global gridded soil information based on machine learning. *PLOS ONE*, **12**, e0169748, https://doi.org/10.1371/journal.pone.0169748.
- Hersbach, H., 2000: Decomposition of the Continuous Ranked Probability Score for
 Ensemble Prediction Systems. Weather and Forecasting, 15, 559–570,
 https://doi.org/10.1175/1520-0434(2000)015<0559:DOTCRP>2.0.CO;2.
- Heuvelink, D., M. Berenguer, C. C. Brauer, and R. Uijlenhoet, 2020: Hydrological application of radar rainfall nowcasting in the Netherlands. *Environment International*, **136**, 105431, https://doi.org/10.1016/j.envint.2019.105431.
- Imhoff, R. O., C. C. Brauer, A. Overeem, A. H. Weerts, and R. Uijlenhoet, 2020: Spatial and
 Temporal Evaluation of Radar Rainfall Nowcasting Techniques on 1,533 Events.
 Water Resources Research, 56, e2019WR026723,
- https://doi.org/10.1029/2019WR026723.
- 836 —, —, K. J. van Heeringen, R. Uijlenhoet, and A. H. Weerts, 2022: Large-Sample
 837 Evaluation of Radar Rainfall Nowcasting for Flood Early Warning. Water Resources
 838 Research, 58, e2021WR031591, https://doi.org/10.1029/2021WR031591.

839	Junghänel, T., and Coauthors, 2021: Hydro-klimatologische Einordnung der Stark- und
840	Dauerniederschläge in Teilen Deutschlands im Zusammenhang mit dem

841 Tiefdruckgebiet "Bernd" vom 12. bis 19. Juli 202. Deutscher Wetterdienst, 16.

842 Kollet, S. J., and R. M. Maxwell, 2006: Integrated surface-groundwater flow modeling: A 843 free-surface overland flow boundary condition in a parallel groundwater flow model.

844 Advances in Water Resources, 29, 945–958,

- 845 https://doi.org/10.1016/j.advwatres.2005.08.006.
- 846 Kreienkamp, F., and Coauthors, 2021: Rapid attribution of heavy rainfall events leading to the severe flooding in Western Europe during July 2021. World Weather Attribution, 847 848 https://www.worldweatherattribution.org/heavy-rainfall-which-ledto-severe-flooding-849 in-western-europe-made-more-likely-byclimate-change
- 850 Kuffour, B. N. O., N. B. Engdahl, C. S. Woodward, L. E. Condon, S. Kollet, and R. M. 851 Maxwell, 2020: Simulating coupled surface–subsurface flows with ParFlow v3.5.0:
- capabilities, applications, and ongoing development of an open-source, massively 852
- parallel, integrated hydrologic model. Geoscientific Model Development, 13, 1373– 853
- 854 1397, https://doi.org/10.5194/gmd-13-1373-2020.
- 855 Langanke, T., M. Steidl, C. Schleicher, and C. Sannier, 2016: Copernicus Land Monitoring 856 Service – High Resolution Layer Imperviousness: Product Specifications Document.
- European Environment Agency, https://land.copernicus.eu/user-corner/technical-857
- library/hrl-imperviousness-technical-document-prod-2015. 858
- 859 Le Bihan, G., O. Payrastre, E. Gaume, D. Moncoulon, and F. Pons, 2017: The challenge of forecasting impacts of flash floods: test of a simplified hydraulic approach and 860 861 validation based on insurance claim data. Hydrology and Earth System Sciences, 21, 5911–5928, https://doi.org/10.5194/hess-21-5911-2017. 862
- 863 Li, L., W. Schmid, and J. Joss, 1995: Nowcasting of motion and growth of precipitation with radar over a complex orography. Journal of Applied Meteorology, 34, 1286–1300, 864 https://doi.org/10.1175/1520-0450(1995)034<1286:NOMAGO>2.0.CO;2. 865
- 866 Lin, C., S. Vasić, A. Kilambi, B. Turner, and I. Zawadzki, 2005: Precipitation forecast skill of numerical weather prediction models and radar nowcasts. Geophysical Research 867 Letters, 32, https://doi.org/10.1029/2005GL023451. 868
- Lovat, A., B. Vincendon, and V. Ducrocq, 2022: Hydrometeorological evaluation of two 869 nowcasting systems for Mediterranean heavy precipitation events with operational 870 871 considerations. Hydrology and Earth System Sciences, 26, 2697–2714, 872 https://doi.org/10.5194/hess-26-2697-2022.
- 873 Maxwell, R. M., 2013: A terrain-following grid transform and preconditioner for parallel, 874 large-scale, integrated hydrologic modeling. Advances in Water Resources, 53, 109– 875 117, https://doi.org/10.1016/j.advwatres.2012.10.001.
- 876 Mejsnar, J., Z. Sokol, and J. Minářová, 2018: Limits of precipitation nowcasting by 877 extrapolation of radar reflectivity for warm season in Central Europe. Atmospheric Research, 213, 288–301, https://doi.org/10.1016/j.atmosres.2018.06.005. 878

879	Merz, B.,	, and	Coauth	ors,	2020:	Impact	Fore	casting to	o Support	Emergency	Management of	of
		_					_					

Natural Hazards. Reviews of Geophysics, **58**, e2020RG000704,

- https://doi.org/10.1029/2020RG000704.
- Mohr, S., and Coauthors, 2023: A multi-disciplinary analysis of the exceptional flood event
- of July 2021 in central Europe Part 1: Event description and analysis. *Natural*
- Hazards and Earth System Sciences, 23, 525–551, https://doi.org/10.5194/nhess-23-
- 885 525-2023.
- Moisselin, J.-M., P. Cau, C. Jauffret, I. Bouissières, and R. Tzanos, 2019: Seamless approach
- for precipitations within the 0-3 hours forecast-interval. *Third European Nowcasting*
- 888 *Conf.*, Madrid, Spain, Agencia Estatal de Meteorologia, 1–17,
- https://hdl.handle.net/20.500.11765/10588.
- 890 Muñoz-Sabater, J., and Coauthors, 2021: ERA5-Land: a state-of-the-art global reanalysis
- dataset for land applications. Earth System Science Data, 13, 4349–4383,
- 892 https://doi.org/10.5194/essd-13-4349-2021.
- Nash, J. E., and J. V. Sutcliffe, 1970: River flow forecasting through conceptual models part I
- A discussion of principles. *Journal of Hydrology*, **10**, 282–290,
- 895 https://doi.org/10.1016/0022-1694(70)90255-6.
- Ochoa-Rodriguez, S., and Coauthors, 2015: Impact of spatial and temporal resolution of
- rainfall inputs on urban hydrodynamic modelling outputs: A multi-catchment
- investigation. *Journal of Hydrology*, **531**, 389–407,
- 899 https://doi.org/10.1016/j.jhydrol.2015.05.035.
- 900 Oudin, L., F. Hervieu, C. Michel, C. Perrin, V. Andréassian, F. Anctil, and C. Loumagne,
- 901 2005: Which potential evapotranspiration input for a lumped rainfall—runoff model?:
- Part 2—Towards a simple and efficient potential evapotranspiration model for
- rainfall–runoff modelling. *Journal of Hydrology*, **303**, 290–306,
- 904 https://doi.org/10.1016/j.jhydrol.2004.08.026.
- Panagos, P., 2006: European Soil Database. *GEO: connexion*, **5**, 32–33.
- Pappenberger, F., H. L. Cloke, D. J. Parker, F. Wetterhall, D. S. Richardson, and J. Thielen,
- 907 2015a: The monetary benefit of early flood warnings in Europe. *Environmental*
- 908 Science & Policy, **51**, 278–291, https://doi.org/10.1016/j.envsci.2015.04.016.
- 909 —, M. H. Ramos, H. L. Cloke, F. Wetterhall, L. Alfieri, K. Bogner, A. Mueller, and P.
- 910 Salamon, 2015b: How do I know if my forecasts are better? Using benchmarks in
- 911 hydrological ensemble prediction. *Journal of Hydrology*, **522**, 697–713,
- 912 https://doi.org/10.1016/j.jhydrol.2015.01.024.
- Poméon, T., N. Wagner, C. Furusho, S. Kollet, and R. Reinoso-Rondinel, 2020: Performance
- of a PDE-Based Hydrologic Model in a Flash Flood Modeling Framework in
- 915 Sparsely-Gauged Catchments. *Water*, **12**, 2157, https://doi.org/10.3390/w12082157.
- 916 Pulkkinen, S., D. Nerini, A. A. Pérez Hortal, C. Velasco-Forero, A. Seed, U. Germann, and
- L. Foresti, 2019: Pysteps: an open-source Python library for probabilistic precipitation

918 919	nowcasting (v1.0). <i>Geoscientific Model Development</i> , 12 , 4185–4219, https://doi.org/10.5194/gmd-12-4185-2019.
920 921 922 923 924	Reinoso-Rondinel, R., M. Rempel, M. Schultze, and S. Trömel, 2022: Nationwide Radar-Based Precipitation Nowcasting—A Localization Filtering Approach and its Application for Germany. <i>IEEE Journal of Selected Topics in Applied Earth Observations and Remote Sensing</i> , 15 , 1670–1691, https://doi.org/10.1109/JSTARS.2022.3144342.
925 926	Rinehart, R. E., and E. T. Garvey, 1978: Three-dimensional storm motion detection by conventional weather radar. <i>Nature</i> , 273 , 287–289, https://doi.org/10.1038/273287a0.
927 928 929	Ruzanski, E., V. Chandrasekar, and Y. Wang, 2011: The CASA Nowcasting System. <i>Journal of Atmospheric and Oceanic Technology</i> , 28 , 640–655, https://doi.org/10.1175/2011JTECHA1496.1.
930 931 932 933	Saadi, M., L. Oudin, and P. Ribstein, 2020: Crossing the rural—urban boundary in hydrological modelling: How do conceptual rainfall—runoff models handle the specificities of urbanized catchments? <i>Hydrological Processes</i> , 34 , 3331–3346, https://doi.org/10.1002/hyp.13808.
934 935 936 937	——, C. Furusho-Percot, A. Belleflamme, JY. Chen, S. Trömel, and S. Kollet, 2023: How uncertain are precipitation and peak flow estimates for the July 2021 flooding event? <i>Natural Hazards and Earth System Sciences</i> , 23 , 159–177, https://doi.org/10.5194/nhess-23-159-2023.
938 939 940	Šálek, M., L. Brezková, and P. Novák, 2006: The use of radar in hydrological modeling in the Czech Republic – case studies of flash floods. <i>Natural Hazards and Earth System Sciences</i> , 6 , 229–236, https://doi.org/10.5194/nhess-6-229-2006.
941 942 943	Schaap, M. G., F. J. Leij, and M. Th. van Genuchten, 2001: rosetta: a computer program for estimating soil hydraulic parameters with hierarchical pedotransfer functions. <i>Journal of Hydrology</i> , 251 , 163–176, https://doi.org/10.1016/S0022-1694(01)00466-8.
944 945 946	Schalge, B., V. Haefliger, S. Kollet, and C. Simmer, 2019: Improvement of surface run-off in the hydrological model ParFlow by a scale-consistent river parameterization. <i>Hydrological Processes</i> , 33 , 2006–2019, https://doi.org/10.1002/hyp.13448.
947 948 949	Seed, A. W., 2003: A Dynamic and Spatial Scaling Approach to Advection Forecasting. <i>Journal of Applied Meteorology and Climatology</i> , 42 , 381–388, https://doi.org/10.1175/1520-0450(2003)042<0381:ADASSA>2.0.CO;2.
950 951 952	Seed, A. W., C. E. Pierce, and K. Norman, 2013: Formulation and evaluation of a scale decomposition-based stochastic precipitation nowcast scheme. <i>Water Resources Research</i> , 49 , 6624–6641, https://doi.org/10.1002/wrcr.20536.
953 954 955	Sokol, Z., J. Mejsnar, L. Pop, and V. Bližňák, 2017: Probabilistic precipitation nowcasting based on an extrapolation of radar reflectivity and an ensemble approach. <i>Atmospheric Research</i> , 194 , 245–257, https://doi.org/10.1016/j.atmosres.2017.05.003.

956 957 958	Speight, L. J., M. D. Cranston, C. J. White, and L. Kelly, 2021: Operational and emerging capabilities for surface water flood forecasting. <i>WIREs Water</i> , 8 , e1517, https://doi.org/10.1002/wat2.1517.
959	UNEP, ed., 1992: World atlas of desertification. Edward Arnold, 69 pp.
960 961 962 963	Vivoni, E. R., D. Entekhabi, R. L. Bras, V. Y. Ivanov, M. P. V. Horne, C. Grassotti, and R. N. Hoffman, 2006: Extending the Predictability of Hydrometeorological Flood Events Using Radar Rainfall Nowcasting. <i>Journal of Hydrometeorology</i> , 7 , 660–677, https://doi.org/10.1175/JHM514.1.
964 965 966 967 968	Winterrath, T., and Coauthors, 2018: Radar climatology (RADKLIM) version 2017.002; gridded precipitation data for Germany: Radar-based gauge-adjusted one-hour precipitation sum (RW). approx. 40 MByte per gzip compressed ascii or binary archive with monthly data, https://doi.org/10.5676/DWD/RADKLIM_RW_V2017.002.
969 970 971 972	Wolfson, M. M., B. E. Forman, R. G. Hallowell, and M. P. Moore, 1999: The Growth and Decay Storm Tracker. <i>8th Conf. on Aviation, Range, and Aerospace Meteorology</i> , Dallas, TX, Amer. Meteor. Soc., 4.3., https://ams.confex.com/ams/99annual/abstracts/1494.htm.
973 974 975	Woo, W., and W. Wong, 2017: Operational Application of Optical Flow Techniques to Radar-Based Rainfall Nowcasting. <i>Atmosphere</i> , 8 , 48, https://doi.org/10.3390/atmos8030048.
976 977 978	Xuan, Y., D. Zhu, P. Triballi, and I. Cluckie, 2014: Forecast uncertainty of a lumped hydrological model coupled with the STEPS radar rainfall nowcasts. International Symposium Weather Radar and Hydrology, Washington DC, USA.
979 980 981 982	Yamazaki, D., D. Ikeshima, J. Sosa, P. D. Bates, G. H. Allen, and T. M. Pavelsky, 2019: MERIT Hydro: A High-Resolution Global Hydrography Map Based on Latest Topography Dataset. <i>Water Resources Research</i> , 55 , 5053–5073, https://doi.org/10.1029/2019WR024873.
983	